Express Polymer Letters Vol.16, No.12 (2022) 1280–1303
Available online at www.expresspolymlett.com
https://doi.org/10.3144/expresspolymlett.2022.93

Reseach article

Carbonaceous adsorbents from polymers-rubber and plastic wastes for adsorption of methylene blue

César Troca-Torrado[1], *María Alexandre-Franco*[1], *Carmen Fernández-González*[1], *Manuel Alfaro-Domínguez*[2], *Vicente Gómez-Serrano*[1*]

[1]Departamento de Química Orgánica e Inorgánica, Facultad de Ciencias, Universidad de Extremadura, 06006 Badajoz, Spain.
[2]Departamento de Ingeniería Mecánica, Energética y de los Materiales, Escuela de Ingenierías Industriales, Universidad de Extremadura, 06006 Badajoz, Spain

Received 10 May 2022; accepted in revised form 26 July 2022

Abstract. The development of carbonaceous adsorbent (CAs) from rubber of used tires (TR), poly(ethylene terephthalate) plastic bottles (PET) and an industrial PP (plastic)-EPDM (rubber) blend (VR) to be used in water discoloration treatment is studied. Not only the three starting materials separately but also mixtures of two- and three-components at the mass ratios of 50/50 and 75/12.5/12.5 for all of them were used. The CAs were first prepared by heat-treatment of materials at 900 °C for 2 h in N_2 and at 850 °C for 2 h in steam and then characterized by X-ray diffraction (XRD), scanning electron microscopy (SEM), adsorption of N_2 at –196 °C, mercury porosimetry, FT-IR spectroscopy and measurement of pH of the point of zero charge (pH_{pzc}), and finally tested as adsorbents of methylene blue (MB) in aqueous solution. The yield of the process of preparation of the CAs is significantly higher with TR and quite similar to PET and VR. It noticeably increases or decreases with material mixtures, presumably because of the interaction of VR with TR and PET during such a process. By using such mixtures, larger developments in surface area and porosity are achieved. S_{BET} is 675 $m^2 \cdot g^{-1}$ for the sample prepared from the 50/50 mixture of PET and VR (M3), whereas for the products of the separated activation of PET and VR in steam it is 248 and 100 $m^2 \cdot g^{-1}$. pH_{pzc} ranges between 5.8 and 11.1. The beneficial effect also concerns the adsorption process of MB. The pseudo-second-order kinetic constant is $2.69 \cdot 10^3$ g·mol·h^{-1} and the Langmuir adsorption capacity is $0.85 \cdot 10^3$ g·mol·h^{-1} for M3.

Keywords: *rubber, recycling, industrial applications, carbonaceous adsorbents, methylene blue adsorption*

1. Introduction

During the last decades, the consumption of polymers has increased steadily worldwide because of the population increase together with the trend of people to progressively improve their living conditions [1]. Polymers are chemical compounds widely used in the manufacture of synthetic industrial materials such as rubbers and plastics, which have a large number of varied applications (*e.g.*, in automobiles and packaging industry) and thereby are produced in very large quantities all over the world. After end-of-life, large amounts of obsolete and downgraded rubber and plastic wastes are unavoidably generated, a significant part of which uncontrollably ends up spreading in the environment where are almost ubiquitously becoming progressively accumulated with time as polymers are practically refractory in nature and thereby non-degradable materials [2, 3] (*i.e.*, some plastic products can take more than 500 years to decompose [4]). In aquatic environments, the release from rubber and plastic leachates of potentially toxic additive chemicals to organisms occurs [5]. Therefore, the aforesaid three polymers-derived waste materials of industrial origin have a

*Corresponding author, e-mail: vgomez@unex.es

strong and very lasting detrimental impact on the environment, which to some extent can be mitigated through proper management in the use of such materials.

Nowadays, the disposal of rubber and plastic waste represents a major environmental issue worldwide because for their reduction the development of environmentally acceptable that are cost-effective technologies is a difficult challenge due to complexities inherent in the reuse of polymers [6]. As the best alternative, recycling was encouraged about a decade ago [7–10]. In fact, from the point of view of energy consumption and environmental issues, polymer recycling is the most efficient way to manage these waste materials [11]. As a result, recycling methods of tire and plastic waste have been frequently reviewed before [11–20]. However, plastic waste to a much larger extent is still not recycled at all but incinerated, land-filled or enters the natural environment [21, 22]. In the case of rubber recycling, as a choice, waste rubber can be blended with thermoplastic resins to produce thermoplastic elastomer compounds but however, these materials show poor mechanical performance [11].

A recycling method for polymer materials is based on their conversion into value-added carbonaceous adsorbents (CAs), such as activated carbon [23–25]. Although the process of preparation of this porous carbon material is an energy-consuming procedure, it advantageously offers the possibility of turning polymer materials into environmentally-friendly products with tuned properties for a wider range of laboratory uses and industrial applications. In addition, such products may be chemically modified and thermally regenerated for the benefit of a longer renewed lifespan. Afterward, as recycling delays rather than avoid final disposal, surplus materials at the end of utility can be ultimately eliminated on a permanent basis only by destructive thermal methods of pyrolysis or combustion, as suggested earlier for plastic waste [21]. However, tire rubber and polyethylene terephthalate plastic as such do not appear to be suitable or very attractive materials for pyrolysis [18] (and refs. therein). In the case of CAs, as compared to their aforementioned rubber and plastic precursors, incineration in relative terms would be a more environmentally friendly and acceptable process because of the mitigated emission of environmental pollutants. Furthermore, hazardous particulate ashes arising from the incineration process of the CAs could be further used, *e.g.*, as a source of inorganic chemical compounds. CAs such as activated carbon are widely used in separation processes of gases, liquids and solutes in solution, such as dies from polluted water [26, 27].

Methylene blue (3,7-bis(dimethylamino)pheno-thiazin-5-ium ion); MB, hereafter), an organic cationic dye with chemical formula $C_{16}H_{18}N_3SCl{\cdot}xH_2O$, is among the most commonly used organic dyes in the textile (*i.e.*, for dying cotton, wood and silk), printing, and pesticide industries [28–30]. As a result, larger amounts of MB-containing wastewater effluents are released from mills with the resulting detrimental impact not only on the water appearance and quality but also on human health [28–33], aquatic organisms [34], and aquatic plants [30]. Therefore, from the point of view of environmental protection, the removal of MB from MB-polluted water effluents is a research subject of current interest. Moreover, MB is well known for its strong adsorption on solids [35], such as carbons [36]. In fact, it is used as a test to estimate properties of activated carbons as the specific surface of pores of dimensions greater than 15 Å [37] and of the mesopores [38] (*i.e.*, pores with widths between ~20 and ~500 Å [39]). Also, MB often serves as a model compound for removing organic contaminants from aqueous solutions [35]. The adsorption of MB on low-cost adsorbents has been reviewed before [38].

In the present study, the development of CAs from rubber of used tires (TR), PET plastic bottles (PET) and an industrial polypropylene plastic (PP)-ethylene propylene diene monomer rubber (EPDM) blend (VR) to be used in water discoloration treatment is investigated. The preparation of porous CAs from TR [40–49] and also from PET [50–56] by the method of physical activation has been studied frequently before. However, as far as to our knowledge, VR has not yet been used as raw material in the production of CAs. By taking into account the presumable lower collection and transportation costs and that thereby the use of material mixtures instead of the various materials separately in the production of the CAs should favorably influence the process economic viability and implementation on an industrial scale, on continuing with our previous work on recycling of polymer wastes [43, 57–60], the development of the CAs has been accomplished not only from TR, PET and VR one by one but also from mixtures of two and three components for comparison

purposes. The CAs are prepared by thermal chemical methods of pyrolysis and steam activation, characterized in terms of morphology and porous texture, and tested as adsorbents of MB in aqueous solution. The adsorption process of MB is studied from the kinetic and equilibrium standpoints.

2. Materials and methods

2.1. Raw materials

As furnished kindly by Recipneu (Sines, Portugal), TR was made up of truck and car rubbers at the 5:95 ratio. As received, TR was already wire-freed, shredded, cryogenically size-reduced and sized, the fraction of particle sizes between 1 and 3 mm being selected for subsequent studies. As a source of post consumed PET, bottles of mineral water (Los Riscos, Badajoz, Spain) for human consumption were employed. VR was provided by Catelsa Cáceres, S.A. Using scissors, PET and VR were progressively size-reduced until pieces smaller than 5 mm were obtained.

In the chemical and thermal study of TR, PET and VR, the elemental analysis (C, H, N, S, $O_{diff.}$) of these materials was carried out in a LECO CHNS-932 analyzer. Also, the ash content was determined by incineration of ≈0.5 g of sample in duplicate at 650 °C for 12 h, using a Selecta muffle furnace (Select-Horn). Table 1 lists the contents of C, H, N, S, $O_{diff.}$ and of ashes obtained for TR, PET and VR.

Table 1. Chemical analyses of TR, PET and VR.

Material	C [wt%]	H [wt%]	N [wt%]	S [wt%]	$O_{diff.}$ [wt%]	Ashes [wt%]
TR	85.1	7.41	0.33	1.81	5.4	7.10
PET	62.9	4.27	0.00	0.00	32.8	0.00
VR	88.0	11.82	0.00	0.37	0.00	0.93

Furthermore, the FT-IR spectra were registered, as described below. Moreover, the materials were heat-treated dynamically between ambient temperature to 900 °C at a heating rate of 10 °C·min^{-1} in helium atmosphere (flow rate = 10 ml·min^{-1}) in a Setaram thermogravimetric system (SETSYS Evolution-16).

2.2. Preparation of the CAs

In the preparation of the CAs, a single stage pyrolysis or activation (*i.e.*, pyrolysis and gasification) process was used. A given starting material or mixture was first heat-treated from ambient temperature to maximum heat treatment temperature (MHTT) at 10 °C·min^{-1} and then soaked at MHTT in flowing N_2 (100 ml·min^{-1}) or in a steam/N_2 atmosphere for 2 h. After heating at MHTT, the system was allowed to cool down to room temperature in N_2 atmosphere and the resulting products were weighted and stored in plastic containers until subsequent use. Pyrolysis was carried out in a horizontal cylindrical electrical furnace (Carbolite, 20-802574). For the steam activation experiments, two in series electrical furnaces were used. One of them served as the steam generation system and the other one as the activation system. The flow rate of liquid water (8 ml·min^{-1}) entering the vapor generation system was controlled with a peristaltic pump (Ismatec, MCP, 7518-10) and steam was carried by a N_2 stream (flow rate = 100 ml·min^{-1}) to the activation system. The materials and heating conditions used in the preparation of the CAs are summarized in Table 2, which also lists yield values and sample codes. Altogether, four series of samples were prepared by pyrolysis of the starting materials (T900, P900 and V900) and by activation of such

Table 2. Preparation of the CAs. Yield values and sample notations.

Starting material [mixture]	Mass ratio [wt%]	Atmosphere	MHTT [°C]	Soaking time [h]	Yield [wt%]	Code
TR		N_2	900	2	40.1	T900
PET		N_2	900	2	17.1	P900
VR		N_2	900	2	18.1	V900
TR		H_2O(v)	850	2	24.1	TS
PET		H_2O(v)	850	2	13.7	PS
VR		H_2O(v)	850	2	12.2	VS
TR/PET	50/50	H_2O(v)	850	2	18.7	M1
TR/VR	50/50	H_2O(v)	850	2	20.4	M2
PET/VR	50/50	H_2O(v)	850	2	11.1	M3
TR/PET/VR	75/12.5/12.5	H_2O(v)	850	2	22.7	M7
PET/TR/VR	75/12.5/12.5	H_2O(v)	850	2	13.2	M8
VR/TR/PET	75/12.5/12.5	H_2O(v)	850	2	14.5	M9

materials and of their mixtures in steam (TS, PS and VS, M1–M3 and M7–M9).

2.3. XRD analysis of CAs

Various CAs were analyzed by XRD in a Bruker D8 ADVANCE diffractometer, provided with a Ge 200 monochromator and using Cu $K\alpha_1$ (λ = 1.5406 Å).

2.4. SEM analysis of CAs

SEM images of selected CAs were obtained with a scanning electron microscope model Quanta 3D FEG (FEI Company), operating in the high vacuum mode under and accelerating voltage ranging from 0.1 to 30 kV and using an Everhart Thornley detector for secondary electrons. In this work, a set of 4 SEM images in randomly chosen particle regions and grains were acquired for each sample at different magnification levels.

2.5. Textural analysis of the CAs

The textural characterization of the samples was carried out by N_2 adsorption at –196 °C and by mercury porosimetry. Routinely, the samples were first oven-dried at 120 °C overnight, allowed to cool down to room temperature in a $CaCl_2$ containing desiccator, and weighed. Then, the isotherms of gas adsorption were determined in a Quantachrome apparatus (Autosorb-1). Approximately, 10 mg of sample was placed in a glass holder and degassed at 250 °C for 12 h, prior to adsorption. The experiments of mercury intrusion were performed in a Pore Master 60-Quantachrome porosimeter, using ~0.3 g of sample.

2.6. Surface chemistry analysis

The FT-IR spectra for the starting materials and selected CAs were recorded on a PerkinElmer Spectrum 100 spectrometer, using CA:KBr pellets. After oven-drying at 120 °C overnight and size-reducing, pellets were prepared using the ratio of sample to KBr (Merck, for spectroscopy) equal to 1:1900, the total mass of the heterogeneous mixture being 238 mg. One KBr pellet of the same mass as the sample pellets was also prepared and its spectrum was used as background. For various CAs, pH_{pzc} was measured using 0.01 M NaCl from (Panreac, 99.5%, for analysis) aqueous solutions at pH 2, 4, 6, 8, 10 or 12. These pH values were fixed with 0.1 M HCl (Panreac, 37%, extra pure) or NaOH (Panreac, 98%) aqueous solutions.

2.7. Adsorption of MB

In the study of the adsorption process, MB (Sigma Aldrich, reagent grade, CAS61-73-4) of M_W = 319.18 g·mol^{-1} was used. Adsorption tests were carried out by the batch procedure, using a 10^{-3} mol·l^{-1} MB aqueous solution (pH = 5.6). Preliminary, the UV-visible spectrum was recorded on a Shimadzu spectrophotometer (Model UV-1800) and from it the wavelength corresponding to the absorbance maximum at 664 nm was chosen for subsequent analyses. Also it was checked that MB is a chemically stable substance in aqueous solution (*i.e.*, after more than 10 d had elapsed, no color and absorbance changes were observed in such a solution) and also that Beer's law is obeyed well for solution concentrations between 10^{-6} and $5\cdot10^{-5}$ mol·l^{-1}. After that, either ≈0.10 g or between ≈0.002 and 0.30 g of adsorbent and 25 ml of MB solution were added to a suit of 25 ml test tubes, which were mounted at once in a Selecta (Unitronic-OR-C) thermostatic shaker bath with water at 25 °C and an agitation of 50 oscillations·min^{-1} and maintained under these conditions for 5 min–12 d or for an equilibration time, which was prefixed after previously carrying out kinetic experiments. Finally, the residual liquid was separated by filtration and eventually analyzed at 664 nm. The adsorption of MB was quantified using the mass balance Equation (1):

$$q = (C_i - C_f)\frac{V}{W} \tag{1}$$

where q stands for the amount of MB adsorbed per unit weight of adsorbent, C_i and C_f are the initial and final concentrations of MB, V is the solution volume [l] and W is the adsorbent weight.

3. Results and discussion

3.1. Analysis of the starting materials

3.1.1. Chemical composition

Data in Table 1 show that TR, PET and VR differ significantly from their elemental and proximate chemical compositions. Thus, the markedly higher contents of carbon and hydrogen by the order VR > > TR > PET and also of sulfur for TR as well as the enhanced oxygen content for PET and ash content for TR are worth mentioning. Conversely, also notice that the contents of sulfur and ashes are zero for PET. The sulfur content of 1.81 wt% for TR is intermediate between 1.0 and 2.6 wt% reported in literature

[62–65]. The much higher content of oxygen for PET than for TR and VR is attributable to the presence of structural ester groups in PET. The ash content of 7.10 wt% for TR is within the wide range of ash contents between 2.50 and 25.2 wt% reported for various types of tires [64]. Furthermore, it is only somewhat higher than the determined ash content of 5.0 wt% for rubber of a truck tire [65].

3.1.2. FT-IR spectroscopy

The FT-IR spectra registered for TR, PET and VR are plotted in Figure 1. The spectrum of TR displays a number of readily visible bands at 3440, 2922, 2854, 1632, 1426, 1086, 788 and 446 cm^{-1}, which are attributable in turn to $\nu_{(O–H)}$ vibrations in H-bonded OH groups, $\nu_{(C–H)_{as}}$ vibrations of $–CH_3$ and/or $–CH_2$ groups, $\nu_{(C–H)s}$ vibrations of $–CH_3$ and/or $–CH_2$ groups, $\nu_{(C=C)}$ vibrations of alkenyl and presumably conjugated C=C groups, $\delta_{(C–H)}$ vibrations of $–CH_3$ and $–CH_2$ groups, $\nu_{(C–O)}$ vibrations of TR additives, $\nu_{(C–S)}$ vibrations and $\nu_{(S–S)}$ vibrations of polysulfide structures [66–68] (abbreviations mean: ν, stretching; δ, bending (in-plane); *s*, symmetric; *as*, asymmetric). In addition to absorption bands originated by $\nu_{(O–H)}$, $\nu_{(C–H)}$ and $\delta_{(C–H)}$ vibrations, the spectrum of PET also shows a strong band at 1718 cm^{-1} that is ascribable to $\nu_{(C=O)}$ vibrations in aromatic ester groups. The bands caused by the $\nu_{(C–O)}$ vibration should appear at lower frequencies between 1350 and 1050 cm^{-1} [68]. Furthermore, the band at 1018 cm^{-1} is likely due to the $\nu_{(C–O)}$ vibration of primary –OH groups and the band at 727 cm^{-1} to p-disubstituted aromatic rings, which absorb between 860 and 780 cm^{-1} [68]. According to the chemical composition of PP/EPDM, the spectrum of VR only displays four stronger peaks at frequencies close to bands registered in the spectrum of TR and that may be assigned therefore to the same bond vibrations of organic atomic groupings as for TR.

3.1.3. Thermal analysis

The thermogravimetric (TG) curves obtained for TR, PET and VR, which are plotted in Figure 2, show that these materials, when are heat-treated from room temperature to 900 °C in helium atmosphere, thermally degrade by devolatilization and as a result the mass of sample greatly decreases, mostly at temperatures below ≈460 °C. At higher temperatures, however, the sample mass hardly undergoes any significant change, especially for TR. The temperature at which the mass of sample starts decreasing noticeably is different for the various materials, being significantly lower by the order TR > VR > PET. Furthermore, from the slope of the TG curves it also follows that the kinetics of the process of thermal degradation is slower for TR than for PET and VR and also, though only very slightly, for VR than for PET. For TR, in fact, the DTG curve (*i.e.*, omitted for the sake of brevity) clearly features two overlapping peaks at 373 and 433 °C, the latter being the stronger one, which were also observed previously not only in manufactured rubber tire samples but also in the major rubber components (*i.e.*, natural rubber, styrene-butadiene-rubber and polybutadiene rubber) [69] and waste tire [70]. The mass loss produced up to ≈460 °C is ≈64 wt% for TR, 81 wt% for PET and 82.5 wt% for VR. The markedly smaller mass loss for TR than for PET and VR can be accounted for by the complex chemical composition of TR, which is made up of not only natural and synthetic polymers

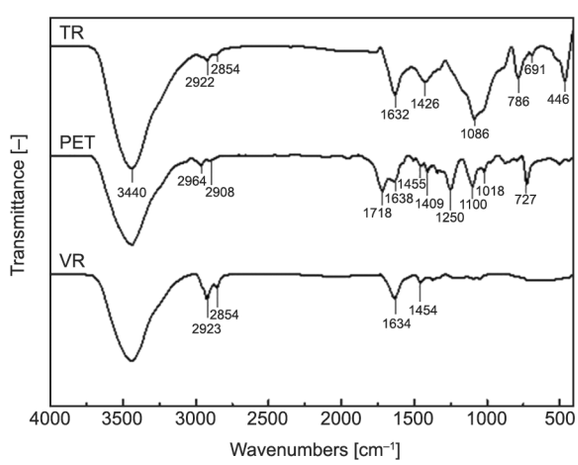

Figure 1. Infrared spectra of TR, PET and VR.

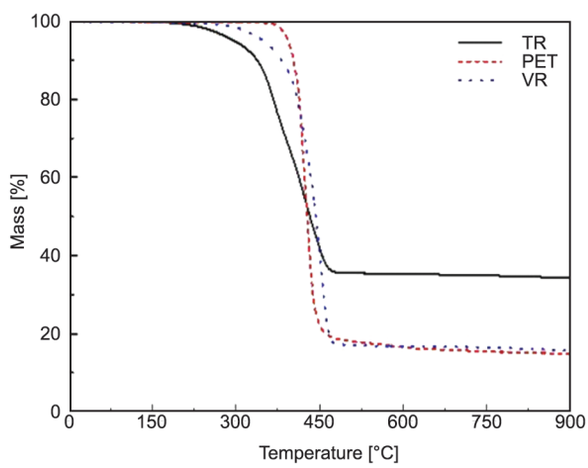

Figure 2. TG analysis of TR, PET and VR.

(elastomers) but also carbon black and a variety of additives, such as sulfur and ZnO that are used as a cross-linking agent and an activator for the vulcanization of rubber, respectively. As a typical composition, tire rubber contains 31.0 wt% of carbon black, 1.1 wt% of sulfur and 1.9 wt% of ZnO [69]. The charcoal residue (34–37%) remaining by heating at 450 °C, at which the whole elastomer is pyrolyzed, includes the initial carbon black, a part of the sulfur and a mixing of sulfur and zinc oxide [71]. In the case of PET, the residue is a black glossy carbon of the equal size to the milled PET feed. The carbon has porous structure and is brittle but very hard [72]. Regarding a PP-EPDM blend, it was also detected the presence of a carbonaceous residue, representing approximately 10% of the initial weight of sample, after heating up to 550 °C in a dynamic TG run [73], in spite of the fact that the thermal degradation of pure PP and EPDM separately at 550 or 700 °C did not result in any char residue [73, 74].

3.2. Preparation and characterization of the CAs

3.2.1. Process yield

In Table 2 the yield values obtained for the sample preparation process are presented. In such a table it is shown first that, regardless of whether the starting materials were used separately or mixed for preparative purposes, yield is markedly higher with TR than with PET and VR and fairly similar with PET and VR. Furthermore, on an average it is 25.1% in N_2 and ≈16.7% in steam, and therefore noticeably higher provided that the starting materials one by one were heat-treated in the former atmosphere, as expected. Moreover, for the three sets of samples activated in steam, *i.e.*, TS, PS and VS, M1–M3, and M7–M9, the same averaged yield of ≈16.7% is obtained. Of course, from these results it may be apparent that the physically mixed TR, PET and VR did not interact with each other during the preparation of the CAs. However, when the aforesaid yield values obtained for M1–M3 and M7–M9 (Table 2) are compared to those assessed from the resulting yield values for TS, PS and VS, weighted by the mass of each material that was used in the preparation of M1–M3 and M7–M9, it is then surprisingly found that the yield of the activation process in steam increases noticeably for M2 (11.0%), M7 (6.1%) and M9 (4.3%) and decreases even more markedly for M3 (–16.7%) and M8 (–12.2%) and only very slightly for M1 (–1.1%).

From the above results of mass balance, it appears likely that VR was the key component of the starting mixture in connection with the changes produced in the mass of sample depending on whether the single materials or material mixtures were used in the preparation of the CAs. Also, it is suggested that during such a treatment VR interacted with TR and PET and that it affected the thermal degradation of these materials. If so, the interaction between mixed materials would become only feasible after the impregnation in part at least of TR and PET by VR. Thus, since the melting temperature is by far lower for PP-EPDM blends [75, 76] than for PET [12, 77]; TR polymers cannot melt because of cross-linking, it can be presumed that during the heat treatment of the mixtures, PP and EPDM melted and impregnated TR and PET pieces. Impregnation should be a more favorable process above 233 °C [77] or 265 °C [12], at which not only PP and EPDM but also PET was in the molten state in the heat-treated heterogeneous mixture. Molten PET will also wet TR. Impregnation might also be promoted because of the greater presence of VR (*i.e.*, 50%, M2 and M3) and of the smaller piece size of TR than of PET in the aforesaid mixture, as suggested by the increase in yield of 4.3% for M9.

As a final comment it should be pointed out that the interaction between PP (plastic) and EPDM (rubber) during heat treatment should not be ruled out. In that connection it has been previously reported when studying the kinetics of the thermal degradation of PP-EPDM blends that the process is not clearly characterized by two independent reactions, suggesting that both components are interacting during degradation [78]. One peak was shown in the derivative TG curve, confirming the existence of a single-step degradation process. For recycled PP-synthetic rubber blends, two peaks were observed however in the dynamic TG tests and the thermal degradation process was completed at 510 °C [73]. According to Gamlin *et al*. [79], PP and EPDM follow complicated random thermal degradation processes.

3.2.2. Chemical composition

Data of the chemical analysis obtained for the starting materials (Table 1) and for selected CAs (Table 3) show that when such materials are heat-treated separately at high temperature in N_2 or in steam atmosphere

strong changes in their chemical constitution occur because of depolymerization and degradation. In general, the carbon content increases, whereas de contents of hydrogen, nitrogen and sulfur decrease, for the prepared CAs. Probably, the great increase originated in the carbon content of P900 and PS is mainly connected with the loss of oxygen from the material during the preparation of the samples. In fact, the oxygen content is equal to 32.8 wt% for PET, 11.94 wt% for P900 and 16.83 wt% for PS. As an exception to the rule, the carbon content is markedly smaller for V900 than for VR, which may be surprising as the residue generated by heat treatment of PP-EPDM is composed of non-polymeric fillers, as seen below. However, notice that the carbon content is similar for VS and VR. On the other hand, the changes produced in the chemical constitution of the materials also depend on the atmosphere used in the preparation of CAs, being less or more drastic for the carbon content and other chemical element contents, respectively. Finally, the carbon content and the hydrogen content are significantly lower for M3 than for PS and VS. It also applies to the hydrogen content for M8 with respect to TS, PS and VS. These results further support the occurrence of interaction between mixed components during the preparation of the samples, which is worth noting.

As shown also in Tables 1 and 3, the sulfur content is higher especially for T900 and TS and also, though less, for V900 and VS; P900 and PS are almost sulfur-free samples. Notice that the sulfur content is even markedly higher for T900 than for TR. These results demonstrate that an important fraction of the original sulfur present in TR is thermally stable and thereby becomes concentrated in the pyrolysis product after the desulfurization of TR. Sulfur compounds thermally decompose into H_2S and/or SO_2 at relatively moderate temperatures [80]. For tire rubber, as Unapumnuk *et al.* [81] report, desulfurization almost completely occurs below 400 °C and reaches the maximum value of ≈65 % at 350 °C and a heating rate of 10 °C/min. Furthermore, the fraction of the original sulfur remaining in the char after desulfurization is approximately half of it between 350 and 850 °C [81] and even as high as between ≈ 60 and 70% at 600–800 °C [82]. It is mainly in the form of non-volatile inorganic sulfides or elemental sulfur, as some trace amounts of organic sulfides, and as ZnS formed by reaction with ZnO [82], as seen in more detail below.

Table 3. Chemical analyses of selected CAs.

Sample	C [wt %]	H [wt %]	N [wt %]	S [wt %]	$O_{diff.}$ [wt %]	Ashes [wt %]
T900	75.1	0.82	0.21	2.74	21.13	15.00
P900	86.2	1.52	0.32	0.02	11.94	0.00
V900	76.7	0.65	0.20	0.72	21.73	0.36
TS	74.8	0.90	0.00	1.51	22.79	22.20
PS	81.5	1.67	0.00	0.00	16.83	1.46
VS	86.5	1.06	0.07	0.61	11.76	14.26
M3	76.1	0.76	0.01	0.25	22.88	6.96
M8	80.5	0.68	0.07	0.35	18.40	10.40

An important quantity of the sulfur found in VR is also thermally stable under the heating conditions and atmospheres used in the preparation of V900 and VS. With respect to 0.37 wt% for VR (Table 1), such an amount is ≈35 % for V900 and ≈20 wt% for VS. Since the thermal degradation of EPDM occurs in a single step below 550 °C with little or no residue [78, 79], the presence of sulfur in the aforementioned samples may be somehow associated with the use of fillers and/or additives in the preparation of VR. In this connection it should be pointed out that, of the sulfur-containing additives typically employed in EPDM formulations, only 2-mercaptobenzothiazole (MBT) is thermally stable in the wide temperature range of 200–900 °C [83]. Although it should be also kept in one's mind that at elevated temperatures desulfurization of EPDM occurs, resulting in shorter sulfur bridges and in the formation of a thiophene-like structure [84]. As far as M3 and M8 is concerned, the sulfur content (*i.e.*, 0.25 and 0.35 wt%, respectively) is markedly lower than for V900 and VS and especially than for T900 and TS. This finding must be highlighted as a reduction in the sulfur content could be the key factor for the industrial application of TR, PET and VR-derived CAs [85].

Although waste tire sulfur is a major prohibiting effective tire disposal [82], from the chemical point of view it may be beneficial with respect to oxygen for specific purposes. Oxygen is another heteroatom almost ubiquitously present in carbonaceous adsorbents, which has been by far the most investigated one, mostly in order to introduce oxygen surface groups to improve the behavior shown by the materials in adsorption and catalysis studies. Because of the larger size of the sulfur atom and ions than of their counterpart oxygen species, according to the well-known hard-soft acid-base theory, the former should interact more favorably with metal ions without d electrons or in a high oxidation state than the

latter. In addition to that, sulfur can be reduced by metals to give sulfide ion, which form water-barely soluble sulfides with numerous metal and semimetal ions of great environmental relevance, such as Hg^{2+}, Pb^{2+}, $As^{3+/5+}$, and so on. Accordingly, it was shown that tire rubber is an efficient sorbent material for Hg^{2+} removal from aqueous solution and that pH is the most crucial of the investigated parameters [86].

The markedly lower ash content (Tables 1 and 3) for M3 and M8 than for TS and VS is due to the dilution of the inorganic matter of TR and VR because of the incorporation of PET to the mixtures used in the preparation of the samples. Typical CAs as activated carbons may contain up to 15 wt% of mineral matter [87].

3.2.3. XRD analysis

The XRD patterns obtained for selected CAs are plotted in Figures 3–5. All of them display a broad peak at $2\theta \approx 25°$ that corresponds to the (002) reflection. The feature of lower intensity at ≈43° is ascribable to the overlapping of the (100) and (101) diffraction peaks [56]. The sharp peaks exhibited by XRD patterns of the samples indicate good crystallinity of the inorganic phases present in the samples. For T900 and TS, Figure 3 shows a large number of such peaks, the position and relative intensity of different combinations of which denoting the presence of hexagonal wurtzite (α-ZnS) [88] and cubic sphalerite (β-ZnS) [89] in T900 and of zincite (ZnO) [90] in TS. The latter peak assignments are supported as well by the standard spectrum for ZnO (JCPDS no. 36-1451). In the case of TS (Figure 3), diffraction peaks attributable to willemite (Zn_2SiO_4) are also readily visible in the XRD pattern (*i.e.*, for peak assignments see [91]). With regard to P900 and PS (Figure 4), by contrast to T900 and TS, no diffraction peak ascribable to Zn crystalline phases is registered in the XRD patterns (*i.e.*, omitted for the sake of brevity), as expected because of the absence of inorganic matter from PET (Table 1). As for V900, VS, M3 and M8 (Figures 4 and 5), the XRD patterns also reveal the presence of ZnO in these CAs. Notice that diffraction peaks are barely visible for V900, unlike for VS, M3 and M8. For these samples, peak intensities vary by the order VS > M3 > > M8, which is in line with the fixed content of VR in the initial mixture used in their preparation. As a final comment it should be pointed out that no diffraction peak at $2\theta \approx 70°$ [92] is shown in the aforementioned diffraction patterns (Figures 3–5) and therefore it becomes apparent that metallic zinc was not formed by reduction of zinc chemical species by carbon when heating at 900 or 850 °C in the preparation of the samples.

As compared to graphite, for which the (002) peak is found at $2\theta = 26.5°$, the shift to $2\theta \approx 25°$ for the CAs indicates an increase in the spacing between the

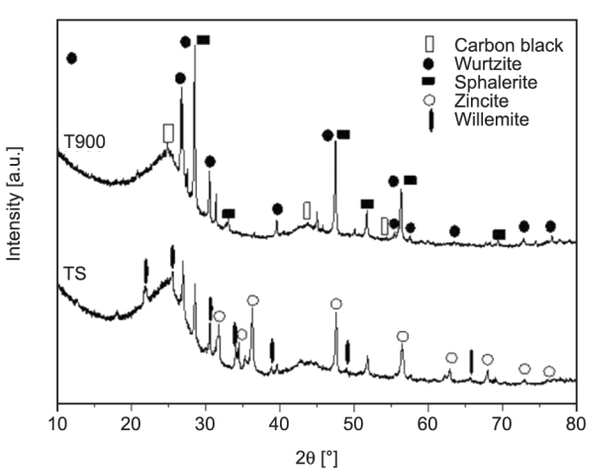

Figure 3. XRD patterns for T900 and TS.

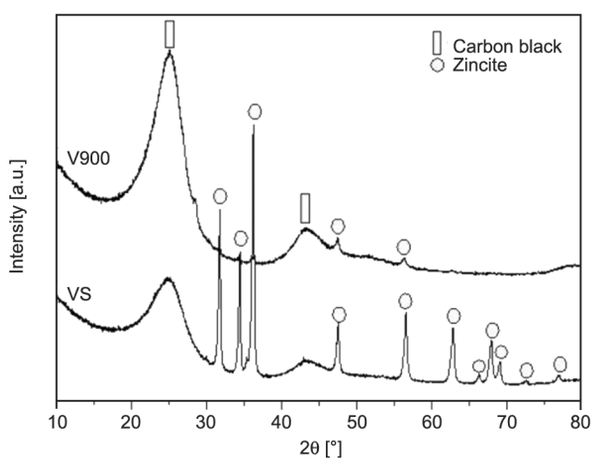

Figure 4. XRD patterns for V900 and VS.

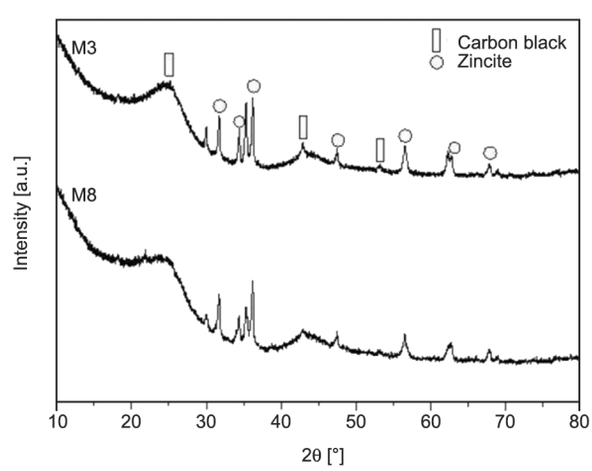

Figure 5. XRD patterns for M3 and V8.

sp^2-layers [93]. On the other hand, the presence of ZnO in a number of CAs is consistent with its use as activator in the process of rubber vulcanization. The formation of Zn-metal sulfide phases was also observed before when studying the pyrolysis of tire rubber [94, 95]. Then, it was stated that most of the ZnO contained in the tires remained ultimately in the char as ZnS [94, 96]. Likewise, Zn appearing on carbon black was found as ZnO below 700 °C [47, 95], whereas above this temperature it was as α- and β-ZnS [97]. Moreover, ZnS was produced by reaction between ZnO and S contained in tires [40, 98]. Although it should be also taken into account that ZnS in the presence of steam may react at high temperature and give ZnO [99] (Equation (2)):

$$ZnS(s) + H_2O(g) = ZnO(s) + H_2S(g); \quad \Delta G^0 = 73.5 \text{ kJ at } 827\,^\circ\text{C} \tag{2}$$

The appearance of Zn_2SiO_4 was associated with the reaction between ZnO and SiO_2 used in the process of tire manufacture. Precipitated SiO_2 is the second most widely used reinforcing filler, after carbon black [100]. Contents of ZnO on an average of 2.95 wt% for two lorry and car tires [85] and of Si ranging between 0.63 and 2.84 wt% for (ash content, 4.7 wt%) ground rubber-derived chars have been reported before [101]. Likewise, according to literature [102], ZnO and SiO_2 react at around 775 °C to form Zn_2SiO_4, which begins to form by solid-diffusion of ZnO from the surface of SiO_2 by the Equation (3):

$$SiO_2(s) + 2ZnO(s) = Zn_2SiO_4(s) \tag{3}$$

3.2.4. Morphological analysis

SEM is commonly applied to observe the morphology of rubber and carbon black composites [103]. In the present study, because of the large number of prepared samples and resulting SEM micrographs of varying magnification, only a few such micrographs will be viewed here for the sake of brevity. The SEM images collected in Figure 6 show a dense mass with isolated cracks and cavities for T900, a very smooth surface with a large number of nearly roundly shaped hollows for P900, and a very rough surface with large cavities and a number of pore mouths ranging widely in size for V900. The SEM micrographs were taken for TS, PS and VS are shown in Figure 7. The micrograph of TS features a fractured surface with wide and deep interconnected cracks and a large number of white color polycrystalline particles which are not uniform in shape and size. These results are consistent with the complex chemical composition of TR since its various components must undergo an unequal expansion and contraction when heated and cooled (*i.e.*, originating cracking and porosity in the resulting product) and also with the fact that very complex and diversiform ZnO particle morphologies and even aggregates have been prepared before [104]. Furthermore, it should be taken into account that the content of inorganic matter is high in TR and that, after the activation treatment of this material in steam, it becomes even more concentrated in TS (*i.e.*, the determined ash content being as high as 22.2% for this sample), and therefore the formation of large size entities as ZnO particle aggregates and agglomerates should not be ruled out. As far as PS is concerned, it is noteworthy that the surface in this sample is somewhat more uneven and the amount of more irregularly shaped hollows is somewhat larger than for P900. As to VS, the surface is more eroded and less steeped than for V900. Also, a very large size cavity and rather isolated and cumulated white color particles are readily visible in the micrograph taken for VS. For M3 and M8, the SEM images in Figure 8 show the presence in these samples of large size hollows or pores, the mouths of which being almost completely full of particulate matter. In the case of M3, however, surface areas with densely crowded and well packed matter are also observed. Particulate matter appears to be loosely held together for M8 and strongly attached to the surface of the carbonaceous substrate for M3. These findings prove that, while heating the mixture of various components in the process of preparation of the samples, VR not only closely contacted PET but also entered porosity created in PET to an extent and in a way depending on the relative content of such components in the starting mixture. However, it should be concomitant with an increased matter release, as commented above in view of the yield values obtained for PET and VR-derived CAs.

3.2.5. Textural characterization of the CAs

N_2 adsorption

The measured adsorption isotherms for the CAs (Figures 9 and 10) by their shape, in general, are composite isotherms of types I or II and IV isotherms of the well-known BDDT classification system. These isotherm shapes have been associated in turn with

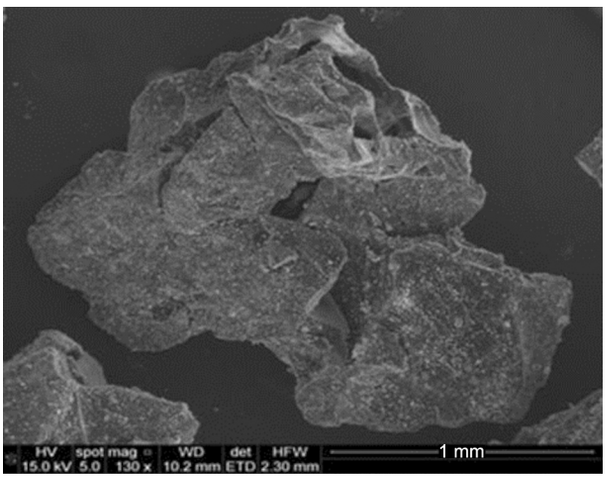

a)

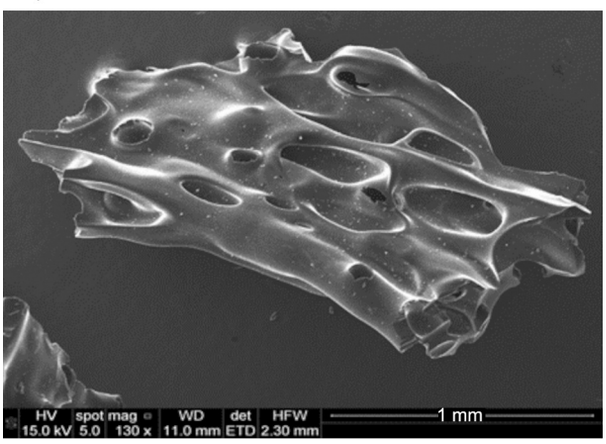

b)

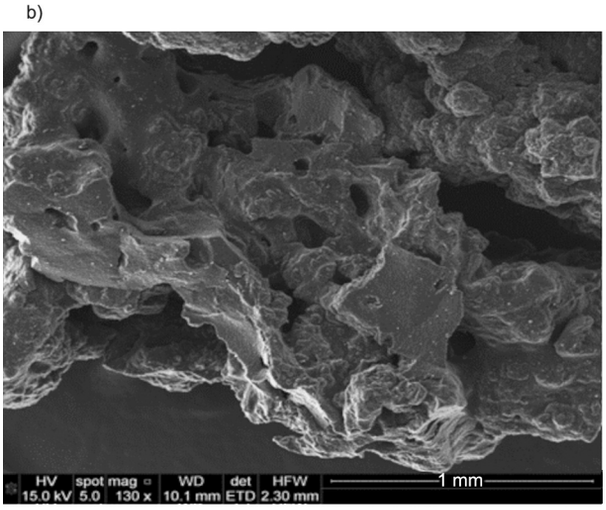

c)

Figure 6. SEM micrographs: a) T900; b) P900; c) V900.

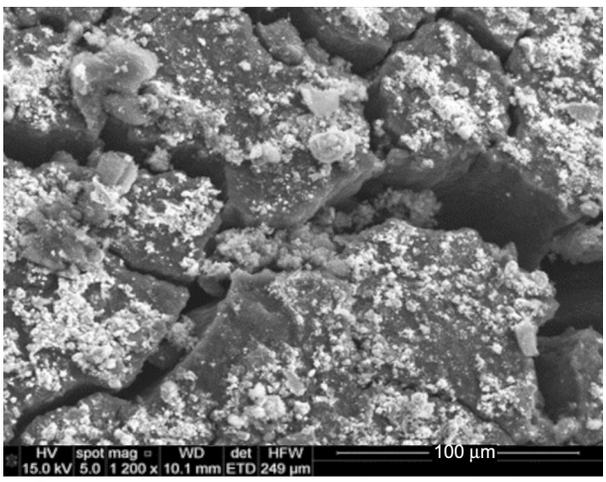

a)

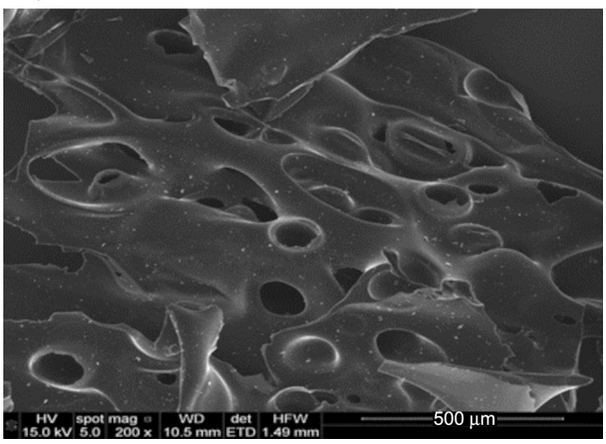

b)

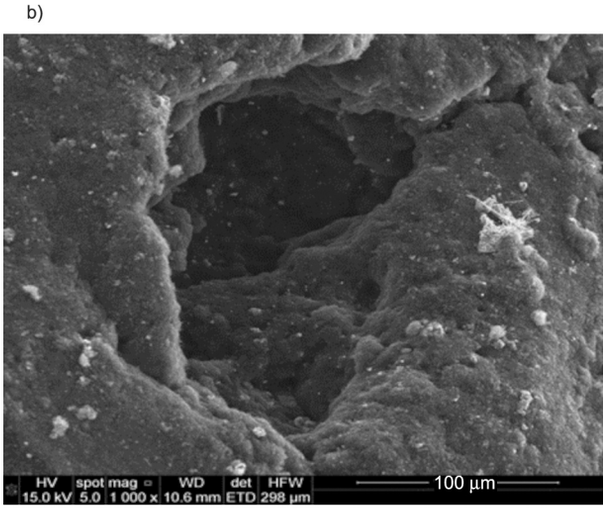

c)

Figure 7. SEM micrographs: a) TS; b) PS; c) VS.

an adsorption mechanism of micropore filling, monolayer-multilayer and monolayer-multilayer-capillary condensation, followed by adsorption systems made up of N_2(g) as adsorptive and microporous, nonporous, and mesoporous solids as adsorbents [39]. In connection with the adsorption of N_2 by tire chars it is worthwhile noting that it was practically reversible under equilibrium, as shown by the relative position of the adsorption and desorption branches in the measured adsorption isotherms [101]. The calculated values of S_{BET}, W_0, V_{mi} and V_{me} from such adsorption isotherms are listed in Table 4. As can be seen, the values S_{BET} and W_0 are very small for T900 and V900. P900 was even non-amenable to the analysis by N_2 adsorption at –196 °C. S_{BET} values reported previously in literature are between 63.0 and

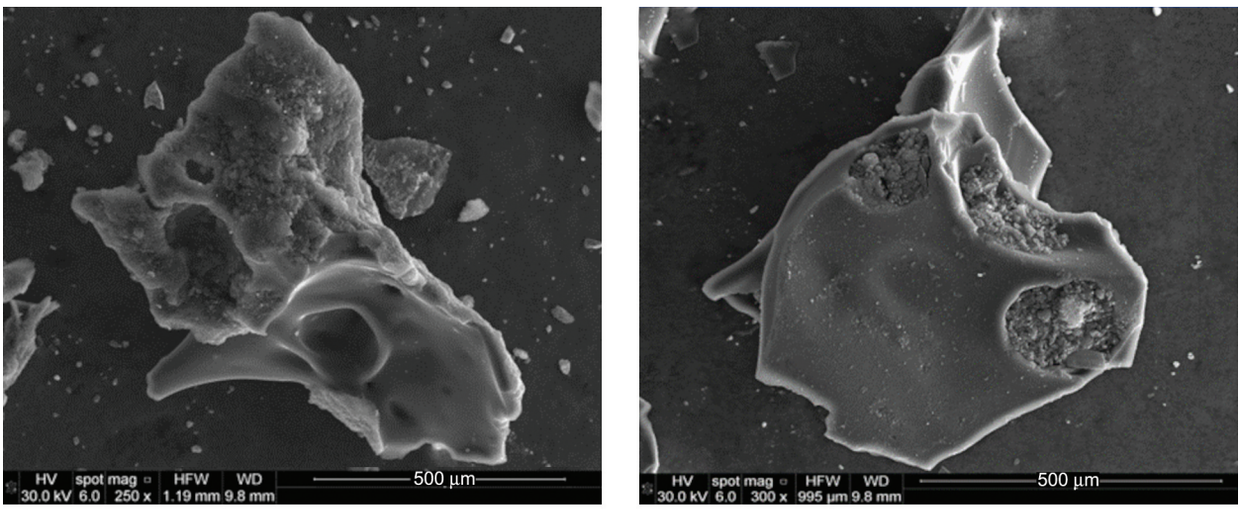

Figure 8. SEM micrographs: a) M3; b) M8.

77.9 $m^2 \cdot g^{-1}$ for a number tire chars prepared at 500–650 °C [105] and equal to 2.44 $m^2 \cdot g^{-1}$ for one char produced by slow pyrolysis of waste PET to a final temperature of 400 °C [106]. Since P900 was heated at a much higher temperature in its preparation from PET, it is possible that shrinkage and even narrowing of pores rather than carbon graphitization occurred, which would account for the absence of measurable microporosity from P900. A significant reduction of porosity was also observed in an early study for olive wood pyrolyzed at 900 and 1000 °C [107]. As compared to the pyrolysis products of TR, PET and VR, S_{BET} and W_0 are markedly higher for the CAs activated in steam. For these products, S_{BET} and W_0 vary by the sequence M3 > M8 > M7 > M1 > TS > M9 > > PS > M2 > VS. Therefore, S_{BET} and W_0 as a rule are higher for the CAs prepared from material mixtures than for those from the individual materials. For the former CAs, S_{BET} and W_0 are especially higher for M3 and M8 and lower for M2 and M9. Only for M2 (*i.e.*, prepared from the 50/50 TR/VR mixture) S_{BET} (153 $m^2 \cdot g^{-1}$) and W_0 (0.11 $cm^3 \cdot g^{-1}$) are even significantly lower than the average values (174 $m^2 \cdot g^{-1}$, 0.13 $cm^3 \cdot g^{-1}$) for TS and VS. In view of these results it may be stated briefly that the effect on S_{BET} and W_0 is usually beneficial or adverse depending on whether the mass of sample, in relative terms as compared to TS, PS and VS, decreased (M3, M8, M1) or increased (M2) in the preparation of the CAs. For M3, S_{BET} and W_0 are as high as 675 $m^2 \cdot g^{-1}$ and 0.39 $cm^3 \cdot g^{-1}$ for M3. For comparison purposes, it is worth mentioning that values of the BET surface area of 302, 640 and 1317 $cm^3 \cdot g^{-1}$ and between 359 and 1235 $cm^3 \cdot g^{-1}$ have been reported before for activated carbons developed from TR [108–110] and PET [59, 111], respectively. Both with TR and PET the preparation of the samples was carried out as usual in two successive carbonization and activation

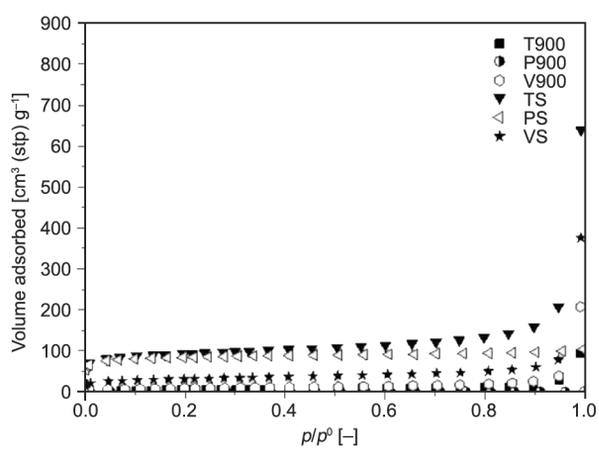

Figure 9. Adsorption isotherms of N_2 at –196 °C for the CAs prepared from single starting materials.

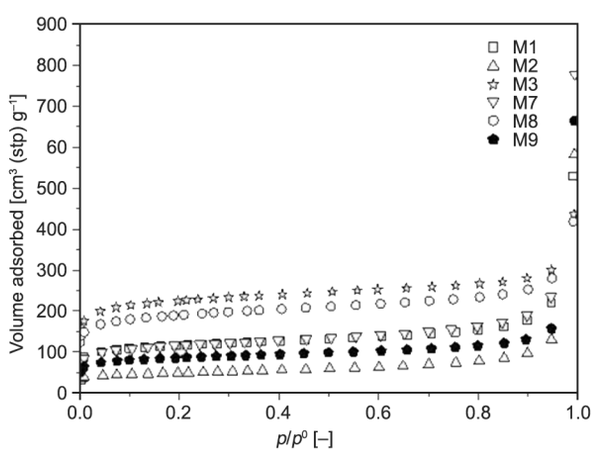

Figure 10. Adsorption isotherms of N_2 at –196 °C for the CAs prepared from material mixtures.

Table 4. Textural data of the CAs. Values of pH_{pzc}.

Sample	S_{BET}[a] [$m^2 \cdot g^{-1}$]	W_0[a] [$cm^3 \cdot g^{-1}$]	V_{mi}[a] [$cm^3 \cdot g^{-1}$]	V_{me}[a] [$cm^3 \cdot g^{-1}$]	$V_{me\text{-}p}$[b] [$cm^3 \cdot g^{-1}$]	$V_{ma\text{-}p}$[b] [$cm^3 \cdot g^{-1}$]	V_T[a,b] [$cm^3 \cdot g^{-1}$]	pH_{pzc}
T900	64	0.05	0.01	0.04	0.35	0.37	0.77	10.4
P900	0	0.00	0.00	0.00	0.07	0.04	0.11	5.8
V900	28	0.02	0.01	0.07	0.05	0.70	0.77	6.9
TS	278	0.19	0.13	0.23	0.32	0.73	1.24	10.3
PS	248	0.14	0.03	0.12	0.02	0.02	0.18	9.3
VS	100	0.07	0.08	0.04	0.01	1.24	1.32	10.1
M1	353	0.22	0.17	0.17	0.18	0.35	0.75	10.5
M2	153	0.11	0.07	0.13	0.19	0.66	0.96	10.6
M3	675	0.39	0.33	0.13	0.15	1.06	1.60	9.4
M7	358	0.23	0.17	0.20	0.31	0.81	1.35	11.1
M8	572	0.34	0.28	0.16	0.18	0.41	0.93	9.8
M9	264	0.17	0.12	0.12	0.08	1.26	1.51	10.6

[a]The N_2 adsorption isotherm: S_{BET}, BET surface area (p/p^0 = 0.05–0.30, am = 16.2 Å^2); W_0 micropore volume (Dubinin-Radushkevich equation [61]); V_{mi}, micropore volume (V_{ad} at p/p^0 = 0.10, V_{ad} = volume adsorbed); V_{me} = mesopore volume (V_{ad} at p/p^0 = 0.95 – V_{ad} at p/p^0 = 0.10). W_0, V_{mi} and V_{me} are expressed as liquid volumes.
[b]Mercury porosimetry: $V_{me\text{-}p}$, mesopore volume; $V_{ma\text{-}p}$ macroporore volume. $V_T = W_0 + V_{me\text{-}p} + V_{ma\text{-}p}$, total pore volume.

stages instead of in a single carbonization stage as in the present study, which would be an advantageous respect from the point of view of process economics. Lastly, as it follows also from Table 4 V_{mi} is usually significantly lower than W_0 and that V_{me} is noticeable higher for TS, M7 and M1, which were prepared either from TR or from TR containing mixtures.

Mercury porosimetry

Mercury porosimetry has been used in the present study as it provides valuable information on porosity (*i.e.*, pore sizes and volumes) of porous solids in the regions of mesopores and macropores. The use of mercury porosimetry in conjunction with gas adsorption in the textural characterization of such solids was earlier suggested if the complete curve of pore volume against pore radius is to be obtained (*i.e.*, the lower limit of the former method is around 35 Å and the upper limit of the latter one is in the region 100–200 Å) [39]. Concerning the pore size and its distribution, as can be seen from Figures 11 and 12, most CAs are essentially macroporous solids. This is especially true for V900, VS, M3 and M9, in which the pores with radii of 2000–250 Å are predominant. Furthermore, macroporosity is quite homogeneous in such samples. In T900, TS, M1, M2 and M7, however, a significant fraction of wide mesopores with pore radii of ≈250–150 Å is also present. Also notice that for a large number of samples, including not only TS but also P900, PS, M1, M3 and M8, the pore-size distribution in the region of mesopores is even wider, embracing smaller pores of varying radius in the range of 150–20 Å. In fact, of all the prepared CAs, TS is the sample that possesses

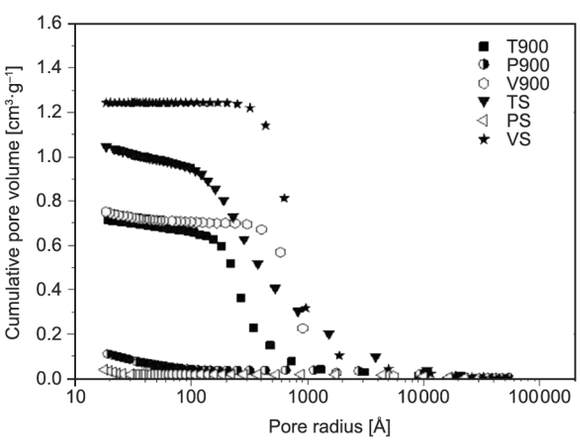

Figure 11. Curves of mercury intrusion for the CAs prepared from single starting materials.

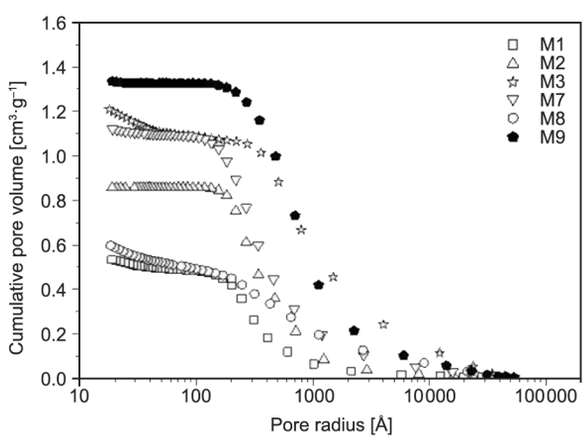

Figure 12. Curves of mercury intrusion for the CAs prepared from material mixtures.

the most heterogeneous porosity, especially in the region of mesopores. Likewise, M3 is the only CA with a high content of different size narrow mesopores. However, the development of macroporosity and mesoporosity is very poor in P900 and PS.

In order to further bring out the textural effects associated with the use of material mixtures as compared to the individual starting materials in the preparation of the CAs, the curves of mercury intrusion obtained for two couples of samples, *i.e.*, VS-M3 and TS-M7, have been potted together in Figure 13, for the sake of clarity. From this figure it becomes evident that by using the material mixtures pore widenings occur, concerning the region of macropores with PET-VR and the region of mesopores with TR-PET-VR. As a final comment it should be mentioned that, regardless of the single materials or material mixtures were used for preparative purposes, the pore size in the aforesaid porosity regions of the resulting CAs is usually larger by VR > TR > PET.

Regarding the pore volumes of the CAs in the regions of mesopores and macropores, Table 4 shows clearly that $V_{ma\text{-}p}$ is much higher than $V_{me\text{-}p}$ for most of the samples. Also, either $V_{me\text{-}p}$ or $V_{ma\text{-}p}$ is a large pore volume for a sample depending on whether individually or mixed TR (T900, TS and M7) or VR (VS, M3, M9, and so on) was used in its preparation. Accordingly, the variation of $V_{me\text{-}p}$ and $V_{ma\text{-}p}$ is usually very wide for the CAs, *e.g.*, see the couple VS-T900 for $V_{me\text{-}p}$ and PS-M9 for $V_{ma\text{-}p}$. However, it is also relevant to point out here that $V_{me\text{-}p}$ is only slightly smaller for TS than for T900 and that $V_{ma\text{-}p}$ is very similar for VR and M9. In short, it may be stated that $V_{me\text{-}p}$ and $V_{ma\text{-}p}$ are strongly dependent on the starting material or mixture and conditions used in the preparation of the samples, as expected simply in view of the curves of mercury intrusion obtained for the CAs (Figures 11–13). As can be also inferred from the values of $V_{me\text{-}p}$ and $V_{ma\text{-}p}$, mesoporosity originates in the pyrolysis of TR and in the activation of all of the PET and VR containing mixtures, whereas macroporosity is generated as a result of the pyrolysis of VR and of the activation of TR and especially of VR and the aforesaid mixtures, *i.e.*, all of mixtures, except for TR-PET and TR-VR. With the latter mixture (sample M2), the effect of macroporosity development was even unfavorable, as revealed by the much lower $V_{ma\text{-}p}$ of 0.66 $cm^3 \cdot g^{-1}$ for M2 than 0.985 $cm^3 \cdot g^{-1}$, which is the average value of $V_{ma\text{-}p}$, as calculated from the determined values of $V_{ma\text{-}p}$ for TS (0.73 $cm^3 \cdot g^{-1}$) and VS (1.24 $cm^3 \cdot g^{-1}$).

According to the values of W_0, $V_{me\text{-}p}$ and $V_{ma\text{-}p}$, as described above, the values of V_T (Table 4) also vary greatly between 0.11 $cm^3 \cdot g^{-1}$ for P900 and 1.60 $cm^3 \cdot g^{-1}$ for M3. In fact, not only W_0 and $V_{ma\text{-}p}$ but also in relative terms $V_{me\text{-}p}$ has a high value for M3. In general, the values of V_T are larger for the samples prepared from VR and from VR and PET containing mixtures: 1.32 $cm^3 \cdot g^{-1}$, VS; 1.51 $cm^3 \cdot g^{-1}$, M9; and so on, which contrast with 0.11 $cm^3 \cdot g^{-1}$ for P900 and 0.18 $cm^3 \cdot g^{-1}$ for PS. Since some of the aforementioned samples were prepared from PET mixtures and the others were only from PET, from the results reported here it is evident the strong beneficial effect of using material mixtures on the total porosity of the samples. Finally, it should be mentioned that for a larger number of samples $V_{me\text{-}p}$ is higher than V_{me}, which is in line with the application of controlled external pressure for mercury intrusion in pores of a porous solid dispersed in mercury.

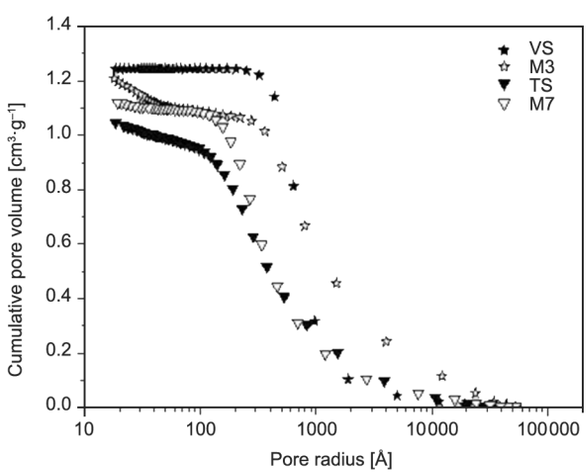

Figure 13. Curves of mercury intrusion for various CAs.

3.2.6. Surface chemistry analysis

FT-IR spectroscopy

The FT-IR spectra registered for selected CAs are plotted in Figure 14. The spectra as a rule display two stronger absorption bands at 3440 and 1637 cm^{-1}. Another relatively strong band is at 1425 cm^{-1} for PS. A series of overlapping weak bands are also shown in the spectra between 1300 and 800 cm^{-1}. Notice the number of such bands is greater for PS and that the broad band at 1056 cm^{-1} is only registered in the spectrum of M8. The aforementioned spectral features are tentatively assigned as shown in Table 5. Since the content of sulfur is high in VS, M3 and M8 (Table 3), in connection with band assignments it is

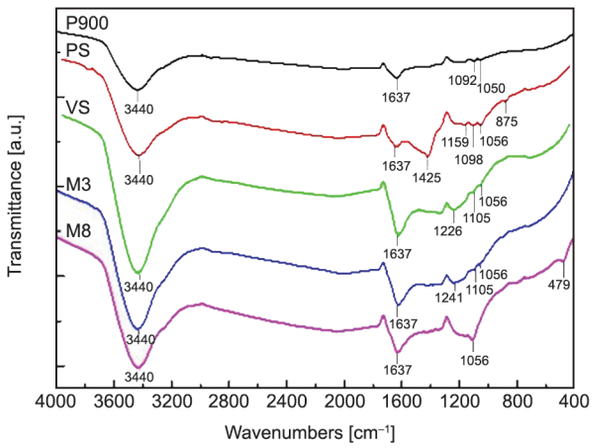

Figure 14. Infrared spectra of selected CAs.

Table 5. FT-IR spectra of selected CAs. Band assignments.

Band position [cm^{-1}]	Assignment	Atomic grouping
3440	$\nu_{(O-H)}$	Water, OH groups
1637	$\delta_{(H-O-H)}$	Water
1425	$\nu_{(C=C)}$	Aromatic rings
1300–1000	$\nu_{(C-O)}$	OH groups
	$\nu_{(C-O-C)}$	Ether structures
	$\nu_{(S-X)}$	Structural S

relevant to point out that the absorption bands due to the $\nu_{(C-S)}$ and $\nu_{(S=O)}$ vibrations appear at 1275–1030 and 1225–980 cm^{-1}, respectively. For the $\nu_{(C-S)}$ and $\nu_{(S-S)}$ vibrations, however, the bands are located at lower frequencies, *i.e.*, 750–550 and ≈500 cm^{-1} [68]. The latter also applies to ZnO, the spectrum of which displays two bands at 545 and 457 cm^{-1} [112]. In any event, from the significantly smaller number of bands showed in the spectra of M3 and M8 than in the spectrum of PS it becomes apparent the dependence of the surface chemistry of CAs on the material or mixtures used in their preparation. The fact that the presence of C=O containing surface structures such as the carboxylic acid functional groups has not been detected in the analyzed CAs is worth mentioning as such groups are usually present in CAs prepared, modified or stored in oxidizing media.

Measurement of pH$_{pzc}$

The pH$_{pzc}$ of adsorbent materials provides valuable information on the acid-base character of their surface, which is relevant in connection with the behavior exhibited by such materials in the adsorption of polar solutes from aqueous solution. The measured values of pH$_{pzc}$ in the present study for the prepared CAs are listed in Table 4. As shown in this table, pH$_{pzc}$ depends strongly on the starting material and mixture as well as atmosphere used in the preparation of the CAs. As a general trend, pH$_{pzc}$ is higher especially with TR and less for VR with respect to PET (*e.g.*, see for the pyrolyzed products). pH$_{pzc}$ ranges widely between 5.8 for P900 and 11.1 for M7. As expected, it is higher for M1, M2, M7 and M9 than for M9 and mostly for M3. Also notice that pH$_{pzc}$ is above 10.0 for a large number of samples. If the values of pH$_{pzc}$ measured for M1–M3 and M7–M9 are compared with the calculated ones from those obtained for TS, PS and VS, it follows then that the former as a rule are significantly higher than the latter. As the only exception to the rule is M3, for which pH$_{pzc}$ is in turn 9.4 and 9.7. This finding deserves to be highlighted because it also corroborates the occurrence of interaction between components of mixtures under the heating conditions used in sample preparation. On the other hand, the use of steam instead of nitrogen originated a marked increase in pH$_{pzc}$ with PET and VR in such a way that pH$_{pzc}$ becomes then fairly similar for TS and VS and only slightly lower for PS. Finally, it should be mentioned that the values of pH$_{pzc}$ determined for the CAs are in line with the absence of carboxylic acid groups from the surface of the analyzed CAs since pH$_{pzc}$ should tend then to increase owing to, as an acid, the –COOH group is stronger than the –OH group.

3.3. Adsorption of MB

3.3.1. Kinetics

The data of concentration of the MB solution (C) as a function of time (t) are plotted in Figures 15 and 16. The kinetic data were fitted to the pseudo-first order rate equation of Lagergren [113] and to the pseudo-second order rate equation of Ho and McKay [114]. The former rearranged to a linear form is usually written as Equation (4):

$$\log(q_e - q_t) = \log q_e - \frac{k_1}{2.303} t \quad (4)$$

with q_e and q_t standing for the amount of MB adsorbed [mol·g^{-1}] at equilibrium and at time t [h], respectively, and k_1 is the rate constant of first order adsorption [h^{-1}]. Therefore, the plot of log($q_e - q_t$) *versus* $_t$ should be a straight line with slope log qe and intercept $-k_1/2.303$.

By assuming that the adsorption capacity is proportional to the number of active sites occupied on the

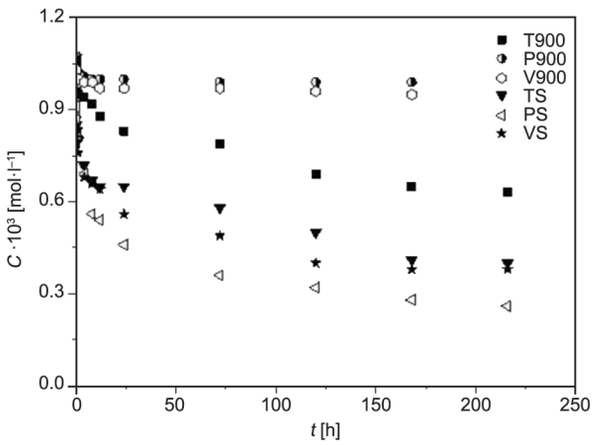

Figure 15. Adsorption kinetics of MB on the CAs prepared from single starting materials.

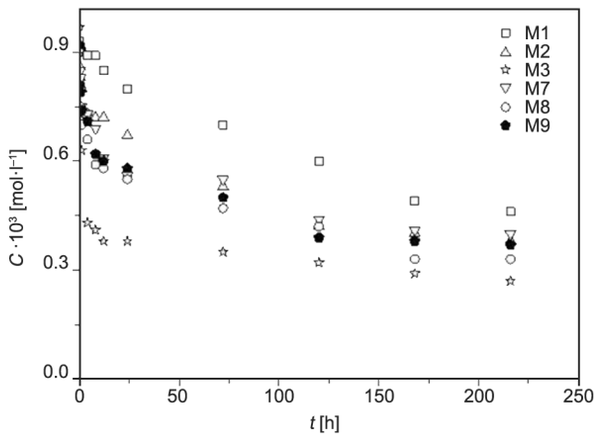

Figure 16. Adsorption kinetics of MB on the CAs prepared from material mixtures.

surface of the adsorbent, the integrated rate law for the pseudo-second order reaction is (Equation (5)):

$$\frac{1}{q_t} = \frac{1}{k_2 q_e^2} + \frac{1}{q_e} t \quad (5)$$

with (Equation (6)):

$$h = k_2 q_e^2 \quad (6)$$

where k_2 [g·mol^{-1}·h^{-1}] is the rate constant of second order adsorption and h is the initial adsorption rate. Here, the plot of t/q_t against t should give a linear relationship, from which q_e and k_2 can be obtained.

The equilibration time (t_e, h) together with the values of q_e, k_1, k_2 and R^2 obtained for the various adsorption systems by using Equations (4) and (5) are given in Table 6. According to the values of R^2, the experimental adsorption data fit better to the pseudo-second order kinetic model than to the pseudo-first order kinetic model. From Figures 9 and 10 and from the values of t_e and k_2 listed in Table 6 it becomes apparent that the kinetics of the adsorption process of MB is faster, especially for P900 and V900 and also, albeit less, for M3 than for the rest of the CAs. The nearly instantaneous adsorption process of MB with P900 and V900 can be accounted for by the almost exclusive presence of meso- and macropores in this couple of CAs (Table 4), as it would make easy the access of MB to surface adsorption active sites of the adsorbent. However, as proved by the very low qe values (Table 6), the content of such active sites was of little significance in the aforementioned samples, probably due to a small degree of microporosity development (*i.e.*, 0.02 cm^3·g^{-1} at most for V900). As far as sample M3 is concerned, the rapid kinetics of MB is consistent with the increased porosity in this sample not only in the regions of macro- and mesopores but also in the region

Table 6. Adsorption kinetics of MB.

Sample	t_e [h]	Pseudo-first-order model			Pseudo-second-order model		
		$q_e \cdot 10^4$ [mol·g^{-1}]	$k_1 \cdot 10^3$ [h^{-1}]	R^2	$q_e \cdot 10^4$ [mol·g^{-1}]	$k_2 \cdot 10^{-3}$ [g·mol^{-1}·h^{-1}]	R^2
T900	120	0.91	13.59	0.968	1.15	0.66	0.960
P900	12	0.08	19.11	0.767	0.19	23.77	0.999
V900	12	0.13	19.81	0.746	0.28	13.63	0.998
TS	168	1.19	16.35	0.854	1.74	0.76	0.976
PS	168	1.25	19.81	0.900	2.00	1.13	0.995
VS	168	1.05	19.58	0.959	1.78	1.14	0.995
M1	168	1.25	12.67	0.938	1.57	0.42	0.943
M2	120	1.18	15.20	0.964	1.81	0.69	0.984
M3	24	0.80	21.88	0.785	1.96	2.69	0.999
M7	168	1.02	17.27	0.923	1.96	1.10	0.991
M8	168	1.09	16.81	0.888	1.87	1.04	0.990
M9	168	1.05	20.04	0.944	1.78	1.17	0.994

of micropores (Figures 10 and 12, Table 4), because of the favorable influence of these textural properties on the processes of diffusion and adsorption of MB.

3.3.2. Adsorption isotherms

The adsorption isotherms measured for MB in aqueous solution and the prepared CAs are plotted in Figures 17 and 18. By their shape, the isotherms seem to belong to the class L of the Giles classification system [115] and thereby MB should adsorb flat on the surface of the adsorbent. Such a MB orientation rather than end-on in micropores of the adsorbent is compatible with the large size of the MB ion because of steric hindrances. Thus, MB in dilute aqueous solution is found in equilibrium between both chemical structures in resonance shown in Figure 19. The approximate dimensions of the monomer are: length, 16 Å; width, 8.4 Å; minimum thickness, 4.7 Å [116, 117] and its reported projected area ranging between 130 and 135 Å^2 [118]. To the flat adsorption of MB

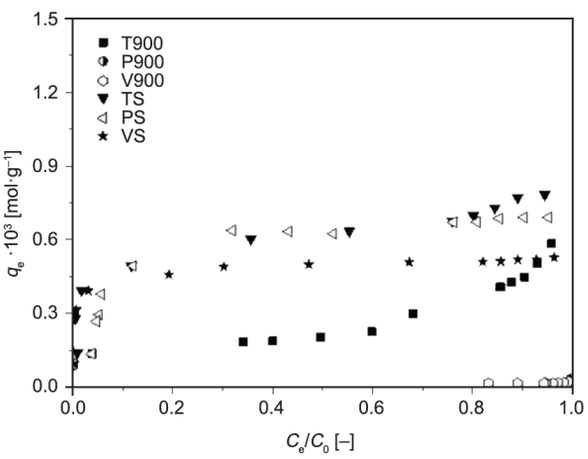

Figure 17. Adsorption isotherms of MB on the CAs prepared from single starting materials.

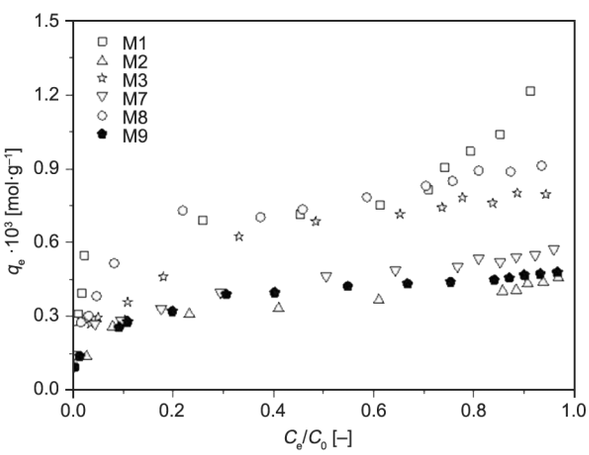

Figure 18. Adsorption isotherms of MB on the CAs prepared from material mixtures.

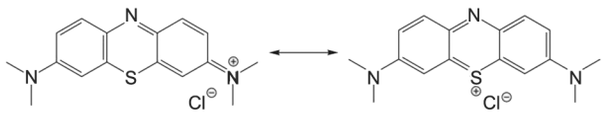

Figure 19. Resonance structures of MB.

could also contribute the π–π dispersive interactions between aromatic rings of the adsorbent surface and the –N=C–C=C system for MB [119]. However, it should be also taken into account that MB is a three-dimensional ion with two dimethylamino groups, supposedly with a trigonal pyramidal geometric shape, which are bonded to carbon atoms of aromatic rings and that should tend to weaken the adsorbate/adsorbent physical interaction or otherwise undergo structural distortion. This statement also applies to the two tetrahedral –CH_3 groups bonded to each nitrogen atom in MB. It is also probable that MB in contact with solvent water molecules in the adsorptive solution is found hydrated on its polar atoms (*i.e.*, S and N atoms with a positive charge or involved in double bonds) and that as a result the end-on disposition of MB on adsorbent surface is not feasible. Moreover, from the values of pH of 5.6 for the MB solution and pH_{pzc} between 5.8 and 11.1 for the CAs (Table 4) it becomes clear that the surface chemistry of the CAs would suffer only very little changes after the MB solution was brought into contact with the solid adsorbents, *i.e.*, the averaged surface charge of a given sample would remain positive up to its corresponding pH_{pzc} value. Therefore, in the absence of hydration, the adsorptive-adsorbent electrostatic forces would prevent the adsorption process involving MB from taking place. Of course, the hydrophobic adsorptive–sorbent interactions occurring in the bulk of the solution would favor the diffusion the adsorptive toward adsorbent adsorption sites. On the other hand, another significant feature of the adsorption isotherms of MB is the great slope of the upward branch defined at low C_e/C_0 values as it denotes a high adsorbent-adsorbate affinity. Also it is the markedly increased adsorption of MB at high C_e/C_0 values with T900, TS and especially M1 that argues for multilayer adsorption.

The adsorption of MB under equilibrium conditions was analyzed by the Langmuir isotherm [120] that in the linear form is (Equation (7)):

$$\frac{C_e}{q_e} = \frac{1}{Q^0 b} + \frac{C_e}{Q^0} \tag{7}$$

In this equation C_e is the equilibrium concentration [mol·l^{-1}], qe is the specific adsorption [mol·l^{-1}], Q^0

is the monolayer adsorption capacity, and b is the constant related to free energy or net enthalpy of adsorption ($b \propto e^{-\Delta H/(RT)}$). Table 7 lists the values of Q^0 and b obtained from the slope and intercept of the plots of $C_e/q_e = f(C_e)$.

As usually written, the Freundlich equation [121] is (Equation (8)):

$$\log q_e = \log K_f + \frac{1}{n} \log C_e \quad (8)$$

where K_f and n are the Freundlich constants, corresponding to adsorption capacity and adsorption intensity. Therefore, the plots of $\log q_e$ against $\log C_e$ should be a straight line with slope $\log K_f$ and intercept $1/n$. The resulting values of K_f and $1/n$ are given in Table 7. The n value indicates the degree of nonlinearity between solution concentration and adsorption, as follows: if $n = 1$, adsorption is linear; if $n < 1$, adsorption is a chemical process; if $n > 1$, adsorption is a physical process. For the adsorption systems under study n is usually higher than 1, which indicates that MB was adsorbed physically by the CAs. It further ranges between 1 and 10, and therefore represents good adsorption of MB [122].

As shown by the values of R^2 listed in Table 7, the adsorption isotherms measured for MB (Figures 17 and 18) as a rule fit well to the Langmuir equation (*i.e.*, R^2 is above 0.990 for a large number of adsorption systems) and noticeably better to such an equation than to the Freundlich equation. Then, according to the assumptions of the Langmuir' equation, it can be assumed that the adsorption of MB from aqueous solution went on with formation of a solute monolayer on a homogeneous surface of the carbon adsorbents.

As can be also seen in such a table, for the various series of samples under study Q^0 is higher for T900, TS and PS, M1 and M3, and M8. Furthermore, it varies by M8 > M3 > M1 > TS > PS ≫ T900. Accordingly, the use especially of materials mixtures with a high content of PET (*i.e.*, 50 or 75%) with VR (50 or 12.5%) and steam atmosphere in the preparation of the CAs favorably influenced the adsorption of MB under equilibrium conditions. The improved behavior shown by M8 and M3 in the adsorption of MB is attributable to the larger degree of microporosity development in such samples. However, the opposite applies to P900, V900, VS, M2, and M9, which were prepared from TR and VR separately and from mixtures with high TR and VR contents. As an exception to the rule it can be noted that Q^0 is also low for M7, despite W_0 being relatively high for this sample (Table 4). Notice that Q^0 is smaller for M7 than for TS, whereas W_0 is significantly larger for the former sample. Perhaps, microporosity of M7 was accessible to the small molecule of N_2(g) at –196 °C in the textural analysis of the samples but not to such a large size chemical species as MB in aqueous solution at 25 °C during the adsorption process of MB. In fact, the size of MB in the bulk of the solution and involved in such a process was likely even increased because of hydration of the MB ion. Textural effects (*e.g.*, porosity narrowing), associated with the increase produced in the mass of sample in the preparation of not only M7 but also of M2 and M9, may also restrict hydrated MB's access to surface active sites of the adsorbent.

The values of Q^0 calculated from the adsorption isotherms of MB and the CAs are usually in the range

Table 7. Adsorption isotherms of MB.

Sample	Langmuir			Freundlich		
	$Q^0 \cdot 10^3$ [mol·g^{-1}]	$b \cdot 10^{-3}$ [l·mol^{-1}]	R^2	$1/n$	$K_f 10^3$ [(mol·g^{-1})/(mol·l^{-1})$^{1/n}$]	R^2
T900	0.22	33.66	0.981	1.11	939.29	0.907
P900	0.00	–0.88	0.897	50.67	∞	0.679
V900	0.02	1.93	0.790	11.44	∞	0.741
TS	0.75	19.77	0.980	0.25	4.10	0.844
PS	0.72	16.00	0.994	0.35	8.08	0.804
VS	0.52	74.41	0.999	0.10	1.06	0.984
M1	0.80	53.74	0.997	0.26	6.05	0.944
M2	0.41	17.57	0.990	0.26	2.60	0.906
M3	0.85	10.13	0.988	0.34	8.34	0.987
M7	0.61	7.12	0.987	0.26	3.24	0.972
M8	0.92	17.41	0.991	0.29	7.06	0.968
M9	0.50	13.00	0.994	0.27	3.04	0.991

Table 8. Preparation of CAs from TR and PET. Langmuir monolayer adsorption capacities for MB from the literature.

Starting material	Preparation method	Q^0 $[mol \cdot g^{-1}] \cdot 10^3$	References
TR	Heat treatment: air, N_2, N_2-steam	0.032, 0.036, 0.092	Jha and Subedi [123]
	Vacuum, 450 °C	0.21	Makrigianni *et al.* [125]
	CO_2, 900 °C, 2 h; $ZnCl_2$, 550 °C, 2 h; Air, 550 °C, 2 h	0.14 0.05 0.11	Shaid *et al.* [126]
	KOH, 1:1, 1:2; N_2, 700 °C	0.011, 0.11	Özbas *et al.* [127]
	N_2, 600 °C; KOH, 1:2, 850 °C, 2 h	0.44	Lian *et al.* [124]
	Steam, 850 °C, 2 h	0.75	This study/TS
PET	N_2, 600 °C; KOH, 1:2, 850 °C, 1.5 h	2.07	Lian *et al.* [124]
	KOH, 1:4, 500 °C, 2 h	1.26	Djahed *et al.* [128]
	PET; K_2CO_3, 0.25-1:1; $ZnCl_2$, 1:1, 500 °C, 2 h	0.36, 0.56-1.95, 1.04	de Castro *et al.* [129]
	Steam, 850 °C, 2 h	0.72	This study/PS

of $0.11 \cdot 10^{-4}$ and $0.44 \cdot 10^{-3}$ $mol \cdot g^{-1}$ brought out for CAs prepared from TR [123–127] or from PET [124, 128, 129] by using different activation methods and heating conditions (Table 8). Nevertheless, it should be noted that as a rule $0.75 \cdot 10^{-3}$ $mol \cdot g^{-1}$ for TS is higher, whereas $0.72 \cdot 10^{-3}$ $mol \cdot g^{-1}$ for PS is lower, than the values of Q^0 found in a literature survey, *i.e.*, $Q^0 = 0.44 \cdot 10^{-3}$ and $2.07 \cdot 10^{-3}$ $mol \cdot g^{-1}$ for CAs developed from TR and PET separately in two successive carbonization and KOH-activation stages, respectively [124]. Likewise, other PET-derived CAs were also prepared by chemical activation with potassium compounds [128, 129] instead of by physical activation in steam as in the present study, which is worth mentioning for comparison purposes. Finally, it should be pointed out that Q^0 was between $4.47 \cdot 10^{-4}$ and $1.42 \cdot 10^{-3}$ $mol \cdot g^{-1}$ for activated carbons produced from a wide variety of materials of vegetable origin [32].

4. Conclusions

From the above results it may be concluded that by using the three starting materials one by one and two- and three material mixtures in the preparation of the CAs, the yields of the pyrolysis and activation processes vary by the order TR ≫ PET ≈ VR. The yield of the activation process in steam either noticeably increases or decreases with the material mixtures as compared to the single materials, being +11.0% for M2 and –16.7% for M3 at most. The fact that M2 and M3 have been prepared from the 50/50 mixtures of VR and TR or PET makes it plausible that VR interacts with TR and PET during such a process, which is further supported by the results obtained in the textural study of the samples and in the adsorption of MB from water.

The use of material mixtures has a marked beneficial effect on the pore texture of CAs. The prepared CAs are mainly macroporous solids with high volumes of mesopores and especially of micropores. For M3 S_{BET} and W_0 are significantly higher (675 $m^2 \cdot g^{-1}$, 0.39 $cm^3 \cdot g^{-1}$) than for PS (248 $m^2 \cdot g^{-1}$, 0.14 $cm^3 \cdot g^{-1}$) and VS (100 $m^2 \cdot g^{-1}$ and 0.07 $cm^3 \cdot g^{-1}$). Narrow mesoporosity is noticeably increased only in M3. Porosity in the regions of mesopores and macropores is more heterogeneous in TS. pH_{pzc} varies between 5.8 and 11.1, being higher than 10.0 for a large number of CAs.

The data of the adsorption of MB fit better to a pseudo-second order kinetics than to a pseudo-first order kinetics and to the Langmuir equation than to the Freundlich equation. The pseudo-second-order kinetic constant (k_2) is $2.69 \cdot 10^{-3}$ $g \cdot mol \cdot h^{-1}$ and the Langmuir adsorption capacity (Q^0) is $0.85 \cdot 10^{-3}$ $mol \cdot g^{-1}$ for M3, and therefore noticeably higher than $1.13 \cdot 10^{-3}$ $g \cdot mol \cdot h^{-1}$ and $0.72 \cdot 10^{-3}$ $mol \cdot g^{-1}$ for PS and 1.14 $g \cdot mol \cdot h^{-1}$ and $0.52 \cdot 10^{-3}$ $mol \cdot g^{-1}$ for VS.

The use of mixed polymer wastes is a very simple method that, only by controlling the composition of the starting heterogeneous mixture, enables to prepare CAs with a tailored porous texture and a significantly improved behavior in the adsorption of MB from aqueous solution.

Acknowledgements

Financial support from the Spanish Ministerio de Ciencia e Innovación through project CTM2008-03636 and from the Junta de Extremadura and European Funds for Regional Development (ERDF) through the aid to Research Groups (GR18013) is gratefully acknowledged.

References

[1] Hamad K., Kaseem M., Deri F.: Recycling of waste from polymer materials: An overview of the recent works. Polymer Degradation and Stability, **98**, 2801–2812 (2013). https://doi.org/10.1016/j.polymdegradstab.2013.09.025

[2] Shah A. A., Hasan F., Hameed A., Ahmed S.: Biological degradation of plastics: A comprehensive review. Biotechnology Advances, **26**, 246–265 (2008). https://doi.org/10.1016/j.biotechadv.2007.12.005

[3] Shah A. A., Hasan F., Shah Z., Kanwal N., Zeb S.: Biodegradation of natural and synthetic rubbers: A review. International Biodeterioration and Biodegradation, **83**, 145–157 (2013). https://doi.org/10.1016/j.ibiod.2013.05.004

[4] Chamas A., Moon H., Zheng J., Qiu Y., Tabassum T., Jang J. H., Abu-Omar M., Scott S. L., Suh S.: Degradation rates of plastics in the environment. ACS Sustainable Chemistry & Engineering, **8**, 3494–3511 (2020).

[5] Capolupo M., Sørensen L., Jayasena K. D. R., Booth A. M., Fabbri E.: Chemical composition and ecotoxicity of plastic and car tire rubber leachates to aquatic organisms. Water Research, **169**, 115270 (2020). https://doi.org/10.1016/j.watres.2019.115270

[6] Burillo G., Clough R. L., Czvikovszky T., Guven O., le Moel A., Liu W., Singh A., Yang J., Zaharescu T.: Polymer recycling: Potential application of radiation technology. Radiation Physics and Chemistry, **64**, 41–51 (2002). https://doi.org/10.1016/S0969-806X(01)00443-1

[7] Stevenson K., Stallwood B., Hart A. G.: Tire rubber recycling and bioremediation: A review. Bioremediation Journal, **12**, 1–11 (2008). https://doi.org/10.1080/10889860701866263

[8] Al-Salem S. M., Lettieri P., Baeyens J.: Recycling and recovery routes of plastic solid waste (PSW): A review. Waste Management, **29**, 2625–2643 (2009). https://doi.org/10.1016/j.wasman.2009.06.004

[9] Ramos G., Aguacil F. J., López Gómez F. A.: The recycling of end-of-life tyres. Technological review. Revista de Metalurgia, **47**, 273–284 (2011). https://doi.org/10.3989/revmetalm.1052

[10] Yazdi M. A., Yang J., Yihui L., Su H.: A review on application of waste tire in concrete. International Journal of Civil and Environmental Engineering, **9**, 1656–1661 (2015). https://doi.org/10.5281/zenodo.1338638

[11] Fazli A., Rodrigue S.: Waste rubber recycling: A review on the evolution and properties of thermoplastic elastomers. Materials, **13**, 782 (2020). https://doi.org/10.3390/ma13030782

[12] Awaja F., Pavel D.: Recycling of PET. European Polymer Journal, **41**, 1453–1477 (2005). https://doi.org/10.1016/j.eurpolymj.2005.02.005

[13] Ignatyev I. A., Thielemans W., Vander Beke B.: Recycling of polymers: A review. ChemSusChem, **7**, 1579–1593 (2014). https://doi.org/10.1002/cssc.201300898

[14] Geyer B., Lorenz G., Kandelbauer A.: Recycling of poly(ethylene terephthalate) – A review focusing on chemical methods. Express Polymer Letters, **10**, 559–586 (2016). https://doi.org/10.3144/expresspolymlett.2016.53

[15] Singh N., Hui D., Singh R., Ahuja I. P. S., Feo L., Fraternali F.: Recycling of plastic solid waste: A state of art review and future applications. Composites Part B, **115**, 409–423 (2017). https://doi.org/10.1016/j.compositesb.2016.09.013

[16] Sathiskumar C., Karthikeyan S.: Recycling of waste tires and its energy storage application of by-products – A review. Sustainable Materials and Technologies, **22**, e00125 (2019). https://doi.org/10.1016/j.susmat.2019.e00125

[17] Schyns Z. O., Shaver M. P.: Mechanical recycling of packaging plastics: A review. Macromolecular Rapid Communications, **42**, 2000415 (2020). https://doi.org/10.1002/marc.202000415

[18] Lange J-P.: Managing plastic waste–sorting, recycling, disposal, and product redesign. ACS Sustainable Chemistry Engineering, **9**, 15722–15738 (2021). https://doi.org/10.1021/acssuschemeng.1c05013

[19] Damayanti, Wu H-S.: Strategic possibility routes of recycled PET. Polymers, **13**, 1475 (2021). https://doi.org/10.3390/polym13091475

[20] Carnier A., de Aberu Aldow V., de Castro A. M.: A comprehensive and critical review on key elements to implement enzymatic PET depolymerization for recycling purposes. Biotechnology Advances, **52**, 107811 (2021). https://doi.org/10.1016/j.biotechadv.2021.107811

[21] Geyer R., Jambeck J. R., Law K. L.: Production, use, and fate of all plastics ever made. Science Advances, **3**, e1700782 (2017). https://doi.org/10.1126/sciadv.1700782

[22] Chamas A., Moon H., Zheng J., Qiu Y., Tabassum T., Jang J. H., Abu-Omar M., Scott S. L., Suh S.: Degradation rates of plastics in the environment. ACS Sustainable Chemistry and Engineering, **8**, 3494–3511 (2020). https://doi.org/10.1021/acssuschemeng.9b06635

[23] Wójtowicz M. A., Serio M. A.: Pyrolysis of scrap tires: Can it be profitable? Chemtech, **26**, 48–53 (1996).

[24] Dias J. M., Alvim-Ferraz M. C., Almeida M. F., Rivera-Utrilla J., Sánchez-Polo M.: Waste materials for activated carbon preparation and its use in aqueous-phase treatment: A review. Journal of Environmental Management, **85**, 833–846 (2007).
https://doi.org/10.1016/j.jenvman.2007.07.031

[25] Bazargan A., Hui C. W., Mckay G.: Porous carbons from plastic waste. in 'Porous carbons – Hyperbranched polymers – Polymer solvation' (eds.: Long T., Voit B., Okay O.) Springer, Berlin Vol. 266, 1–26 (2015).
https://doi.org/10.1007/12_2013_253

[26] Ioannidou O., Zabaniotuo A.: Agricultural residues as precursors for activated carbon production – A review. Renewable and Sustainable Energy Reviews, **11**, 1966–2005 (2007).
https://doi.org/10.1016/j.rser.2006.03.013

[27] Tadda M. A., Ahsan A., Shitu A., ElSergany M., Arunkumar T., Jose B., Razzaque M. A., Daud N. N. N.: A review on activated carbon: Process, application and prospects. Journal of Advanced Civil Engineering Practice and Research, **2**, 7–13 (2016).

[28] Rafatullah M., Sulaiman O., Hashim R., Ahmad A.: Adsorption of methylene blue on low-cost adsorbents: A review. Journal of Hazardous Materials, **177**, 70–80 (2010).
https://doi.org/10.1016/j.jhazmat.2009.12.047

[29] Dod R., Banerjee G., Saini S.: Adsorption of methylene blue using green pea peels (*Pisum sativum*): A cost-effective option for dye-based wastewater treatment. Biotechnololy and Bioprocess Engineering, **17**, 862–874 (2012).
https://doi.org/10.1007/s12257-011-0614-5

[30] Kosswattaarachchi A. M., Cook T. R.: Repurposing the industrial dye methylene blue as an active component for redox flow batteries. ChemElectroChem, **5**, 3437–3442 (2018).
https://doi.org/10.1002/celc.201801097

[31] Lorenc-Grabowska E., Gryglewicz G.: Adsorption characteristics of congo red on coal-based mesoporous activated carbon. Dyes and Pigments, **74**, 34–40 (2007).
https://doi.org/10.1016/j.dyepig.2006.01.027

[32] Hameed B. H., Din A. T. M., Ahmad A. L.: Adsorption of methylene blue onto bamboo-based activated carbon: Kinetics and equilibrium studies. Journal of Hazardous Materials, **141**, 819–825 (2007).
https://doi.org/10.1016/j.jhazmat.2006.07.049

[33] Lyu H., Gao B., He F., Zimmerman A. R., Ding C., Tang J., Crittenden J. C.: Experimental and modeling investigations of ball-milled biochar for the removal of aqueous methylene blue. Chemical Engineering Journal, **335**, 110–119 (2018).
https://doi.org/10.1016/j.cej.2017.10.130

[34] Pereira L., Alves M.: Dyes–environmental impact and remediation. in 'Environmental protection strategies for sustainable development' (eds: Malik A., Grohmann E.) Springer, Dordrecht, 111–162 (2012).
https://doi.org/10.1007/978-94-007-1591-2_4

[35] Salman J. M.: Preparation of mesoporous-activated carbon from branches of pomegranate trees: Optimization on removal of methylene blue using response surface methodology. Journal of Chemistry, **2013**, 489670 (2013).
https://doi.org/10.1155/2013/489670

[36] Kannan N., Sundaram M. M.: Kinetics and mechanism of removal of methylene blue by adsorption on various carbons-A comparative study. Dyes and Pigments, **51**, 25–40 (2011).
https://doi.org/10.1016/S0143-7208(01)00056-0

[37] Jankowska H., Swiatkowski A., Choma J.: Active carbon. Horwood, West Sussex (1991).

[38] Adibfar M., Kaghazchi T., Asasian N., Soleimani M.: Conversion of poly(ethylene terephthalate) waste into activated carbon: Chemical activation and characterization. Chemical Engineering and Technology, **37**, 979–986 (2014).
https://doi.org/10.1002/ceat.201200719

[39] Gregg S. J., Sing K. S. W.: Adsorption, surface area and porosity. Academic Press, London (1982).

[40] Teng H., Serio M. A., Wojtowicz M. A., Bassilakis R., Solomon P. R.: Reprocessing of used tires into activated carbon and other products. Industrial and Engineering Chemistry Research, **34**, 3102–3111 (1995).
https://doi.org/10.1021/ie00048a023

[41] Lehmann C. M. B., Rostam-Abadi M., Rood M. J., Sun J.: Reprocessing and reuse of waste tire rubber to solve air-quality related problems. Energy Fuels, **12**, 1095–1099 (1998).
https://doi.org/10.1021/ef9801120

[42] San Miguel G., Fowler G. D., Sollars C. J.: Pyrolysis of tire rubber: Porosity and adsorption characteristics of the pyrolytic chars. Industrial and Engineering Chemistry Research, **37**, 2430–2435 (1998).
https://doi.org/10.1021/ie970728x

[43] Manchón-Vizuete E., Macías-García A., Gisbert N. A., Fernández-González C., Gómez-Serrano V.: Preparation of mesoporous and macroporous materials from rubber of tyre wastes. Microporous and Mesoporous Materials, **67**, 35–41 (2004).
https://doi.org/10.1016/j.micromeso.2003.10.002

[44] Zabaniotou A., Madau P., Oudenne P. D., Jung C. G., Delplancke M-P., Fontana A.: Active carbon production from used tire in two-stage procedure: Industrial pyrolysis and bench scale activation with H_2O-CO_2 mixture. Journal of Analytical and Applied Pyrolysis, **72**, 289–297 (2004).
https://doi.org/10.1016/j.jaap.2004.08.002

[45] Murillo R., Navarro M. V., García T., López J. M., Callén M. S., Aylón E., Mastral A. M.: Production and application of activated carbons made from waste tire. Industrial and Engineering Chemistry Research, **44**, 7228–7233 (2005).
https://doi.org/10.1021/ie050506w

[46] López G., Olazar M., Artetxe M., Amutio M., Elordi G., Bilbao J.: Steam activation of pyrolytic tyre char at different temperatures. Journal of Analytical and Applied Pyrolysis, **85**, 539-543 (2009). https://doi.org/10.1016/j.jaap.2008.11.002

[47] López F. J., Centeno T. A., Aguacil F. J., Lobato B., López-Delgado A., Fermoso J.: Gasification of the char derived from distillation of granulated scrap tyres. Waste Management, **32**, 743–752 (2012). https://doi.org/10.1016/j.wasman.2011.08.006

[48] Heras F., Alonso-Morales N., Jimenez-Cordero D., Gilarranz M. A., Rodriguez J. J.: Granular mesoporous activated carbons from waste tires by cyclic oxygen chemisorption-desorption. Industrial and Engineering Chemistry Research, **51**, 2609–2614 (2012). https://doi.org/10.1021/ie201499h

[49] Saleh T. A., Danmaliki G. I.: Influence of acidic and basic treatments of activated carbon derived from waste rubber tires on adsorptive desulfurization of thiophenes. Journal of the Taiwan Institute of Chemical Engineers, **60**, 460–468 (2016). https://doi.org/10.1016/j.jtice.2015.11.008

[50] Kartel' K. T., Gerasimenko N. V., Tsyba N. N., Nikolaichuk A. D., Kovtun G. A.: Synthesis and study of carbon sorbent prepared from polyethylene terephthalate. Russian Journal of Applied Chemistry, **74**, 1765–1767 (2001). https://doi.org/10.1023/A:1014894211046

[51] Parra J. B., Ania C. O., Arenillas A., Rubiera F., Pis J. J.: High value carbon materials from PET recycling. Applied Surface Science, **238**, 304–308 (2004). https://doi.org/10.1016/j.apsusc.2004.05.229

[52] Fernández-Morales I., Almazán-Almazán M. C., Pérez-Mendoza M., Domingo-García M., López-Garzón F. J.: PET as precursor of microporous carbons: Preparation and characterization. Microporous and Mesoporous Materials, **80**, 107–115 (2005). https://doi.org/10.1016/j.micromeso.2004.12.006

[53] Przepiórski J., Karolczyk J., Takeda K., Tsumura T., Toyoda M., Morawski A. W.: Porous carbon obtained by carbonization of PET mixed with basic magnesium carbonate: Pore structure and pore creation mechanism. Industrial and Engineering Chemistry Research, **48**, 7110–7116 (2009). https://doi.org/10.1021/ie801694t

[54] Lorenc-Grabowska E., Gryglewicz G., Machnikowski J., Díez M-A., Barriocanal C.: Activated carbons from coal/pitch and polyethylene terephthalate blends for the removal of phenols from aqueous solutions. Energy Fuels, **23**, 2675–2683 (2009). https://doi.org/10.1021/ef801045k

[55] Esfandiari A., Kaghazchi T., Soleimani M.: Preparation and evaluation of activated carbons obtained by physical activation of polyethyleneterephthalate (PET) wastes. Journal of the Taiwan Institute of Chemical Engineers, **43**, 631–637 (2012). https://doi.org/10.1016/j.jtice.2012.02.002

[56] Bratek W., Świątkowski A., Pakuła M., Biniak S., Bystrzejewski M., Szmigielski R.: Characteristics of activated carbon prepared from waste PET by carbon dioxide activation. Journal of Analytical and Applied Pyrolysis, **100**, 192–198 (2013). https://doi.org/10.1016/j.jaap.2012.12.021

[57] Troca-Torrado C., Alexandre-Franco M., Fernández-González C., Alfaro-Domínguez M., Gómez-Serrano V.: Development of adsorbents from used tire rubber: Their use in the adsorption of organic and inorganic solutes in aqueous solution. Fuel Processing Technology, **92**, 206–212 (2011). https://doi.org/10.1016/j.fuproc.2010.03.007

[58] Alexandre-Franco M., Fernández-González C., Alfaro-Domínguez M., Gómez-Serrano V.: Adsorption of cadmium on carbonaceous adsorbents developed from used tire rubber. Journal of Environmentat Management, **92**, 2193–2200 (2011). https://doi.org/10.1016/j.jenvman.2011.04.001

[59] Mendoza-Carrasco R., Cuerda-Correa E. M., Alexandre-Franco M. F., Fernández-González C., Gómez-Serrano V.: Preparation of high-quality activated carbon from polyethyleneterephthalate (PET) bottle waste. Its use in the removal of pollutants in aqueous solution. Journal of Environmental Management, **181**, 522–535 (2016). https://doi.org/10.1016/j.jenvman.2016.06.070

[60] Gómez-Serrano V., Adame-Pereira M., Alexandre-Franco M., Fernández-González C.: Adsorption of bisphenol A by activated carbon developed from PET waste by KOH activation. Environmental Science and Pollution Research, **28**, 24342–24354 (2021). https://doi.org/10.1007/s11356-020-08428-6

[61] Dubinin M. M.: Physical adsorption of gases and vapors in micropores. in 'Progress in surface and membrane science' (eds: Cadenhead D. A., Danielli J. F., Rosenberg M. D) Academic Press, New York, 1–70 (1975). https://doi.org/10.1016/B978-0-12-571809-7.50006-1

[62] Williams P. T., Besler S., Taylor D. T.: The pyrolysis of scrap automotive tyres: The influence of temperature and heating rate on product composition. Fuel, **69**, 474–482 (1990). https://doi.org/10.1016/0016-2361(90)90193-T

[63] Kwon E., Castaldi M. J.: Fundamental understanding of the thermal degradation mechanisms of waste tires and their air pollutant generation in a N_2 atmosphere. Environmental Science and Technology, **43**, 5996–6002 (2009). https://doi.org/10.1021/es900564b

[64] Amari T., Themelis N. J., Wernick I. K.: Resource recovery from used rubber tires. Resources Policy, **25**, 179–188 (1999). https://doi.org/10.1016/S0301-4207(99)00025-2

[65] Larsen M. B., Schultz L., Glarborg P., Skaarup-Jensen L., Dam-Johansen K., Frandsen F., Henriksen U.: Devolatilization characteristics of large particles of tyre rubber under combustion conditions. Fuel, **85**, 1335–1345 (2006). https://doi.org/10.1016/j.fuel.2005.12.014

[66] Macías-García A., Valenzuela-Calahorro C., V. Gómez-Serrano V.: Adsorption of Pb^{2+} by heat-treated and sulfurized activated carbon. Carbon, **31**, 1249–1255 (1993). https://doi.org/10.1016/0008-6223(93)90083-M

[67] Coates J.: Interpretation of infrared spectra, a practical approach. in 'Encyclopedia of analytical chemistry' (ed.: Meyers R. A.) Wiley, Chichester, 10815–10837 (2000). https://doi.org/10.1002/9780470027318.a5606

[68] Badertscher M., Bühlmann P., Pretsch E.: Structure determination of organic compounds. Tables of spectral data. Springer, Berlin (2009). https://doi.org/10.1007/978-3-540-93810-1

[69] Williams P. T., Besler S.: Pyrolysis-thermogravimetric analysis of tyres and tyre components. Fuel, **74**, 1277–1283 (1995). https://doi.org/10.1016/0016-2361(95)00083-H

[70] Singh S., Wu C., Williams P. L.: Pyrolysis of waste materials using TGA-MS and TGA-FTIR as complementary characterisation techniques. Journal of Analytical and Applied Pyrolysis, **94**, 99–107 (2012). https://doi.org/10.1016/j.jaap.2011.11.011

[71] Bouvier J. M., Clin F.: Pyrolysis of rubber and tyres waste. Commission des Communautés Européennes, Report du B.R.G.M., 85 DAM 029 MIN, 1–91 (1985).

[72] Brems A., Baeyens J., Vandecasteele C., Dewil R.: Polymeric cracking of waste polyethylene terephthalate to chemicals and energy. Journal of the Air and Waste Management Association, **61**, 721–731 (2011). https://doi.org/10.3155/1047-3289.61.7.721

[73] Navarro R., Torre L., Kenny J. M., Jiménez A.: Thermal degradation of recycled polypropylene toughened with elastomers. Polymer Degradation and Stability, **8**, 279–290 (2003). https://doi.org/10.1016/S0141-3910(03)00222-2

[74] Tang G., Hu Y., Song L.: Study on the flammability and thermal degradation of a novel intumescent flame retardant EPDM composite. Procedia Engineering, **62**, 371–376 (2013). https://doi.org/10.1016/j.proeng.2013.08.078

[75] Naskar K., Gohs U., Wagenknecht U., Heinrich G.: PP-EPDM thermoplastic vulcanisates (TPVs) by electron induced reactive processing. Express Polymer Letters, **3**, 677–683 (2009). https://doi.org/10.3144/expresspolymlett.2009.85

[76] Brostow W., Datashvili T., Geodakyan J., Lou J.: Thermal and mechanical properties of EPDM/PP + thermal shock-resistant ceramic composites. Journal of Materials Science, **46**, 2445–2455 (2011). https://doi.org/10.1007/s10853-010-5091-2

[77] Silva E., Fedel M., Deflorian F., Cotting F., Lins V.: Properties of post-consumer polyethylene terephthalate coating mechanically deposited on mild steels. Coatings, **9**, 28 (2019). https://doi.org/10.3390/coatings9010028

[78] López-Manchado M., Torre L., Kenny J. M.: Kintic analyis of the thermal degradation of PP-EPDM blends. Rubber Chemistry and Technology, **73**, 694–705 (2000). https://doi.org/10.5254/1.3547614

[79] Gamlin C., Dutta N., Roy-Choudhury N., Kehoe D., Matisons J.: Influence of ethylene–propylene ratio on the thermal degradation behaviour of EPDM elastomer. Thermochimica Acta, **367–368**, 185–193 (2001). https://doi.org/10.1016/S0040-6031(00)00668-7

[80] Meyer R. A.: Coal desulfurization. Marcel Dekker, New York (1977).

[81] Unapumnuk K., Keener T. C., Lu M., Liang F.: Investigation into the removal of sulfur from tire derived fuel by pyrolysis. Fuel, **87**, 951–956 (2008). https://doi.org/10.1016/j.fuel.2007.05.036

[82] Susa D., Haydary J.: Sulphur distribution in the products of waste tire pyrolysis. Chemical Papers, **67**, 1521–1526 (2013). https://doi.org/10.2478/s11696-012-0294-4

[83] Sanches N. B., Cassu S. N., Diniz M. F., Dutra R. C. L.: Characterization of additives typically employed in EPDM formulations by using FT-IR of gaseous pyrolyzates. Polímeros, **24**, 269–275 (2014). https://doi.org/10.4322/polimeros.2014.066

[84] van Duin M.: Chemistry of EPDM cross-linking. Kautschuk Gummi Kunststoffe, **55**, 150–156 (2002).

[85] Lopez G., Olazar M., Amutio M., Aguado R., Bilbao J.: Influence of tire formulation on the products of continuous pyrolysis in a conical spouted bed reactor. Energy Fuels, **23**, 5423–5431 (2009). https://doi.org/10.1021/ef900582k

[86] Knocke W. R., Hemphill L. H.: Mercury(II) sorption by waste rubber. Water Research, **15**, 275–282 (1981). https://doi.org/10.1016/0043-1354(81)90121-4

[87] Rodríguez-Reinoso F.: The role of carbon materials in heterogeneous catalysis. Carbon, **36**, 159–175 (1998). https://doi.org/10.1016/S0008-6223(97)00173-5

[88] Kim Y., Jang D-J.: Facile one-step hydrothermal fabrication of single-crystalline ZnS nanobelts with narrow band-edge luminescence. RSC Advances, **3**, 16945–16948 (2013). https://doi.org/10.1039/c3ra42401d

[89] Cruz-Vázquez C., Rocha-Alonzo F., Burruel-Ibarra S. E., Barboza-Flores M., Bernal R., Inoue M.: A new chemical bath deposition method for fabricating ZnS, $Zn(OH)_2$, and ZnO thin films, and the optical and structural characterization of these materials. Applied Physics A, **79**, 1941–1945 (2004). https://doi.org/10.1007/s00339-003-2097-5

[90] Prabhu Y. T., Rao K. V., Kumar V. S. S., Kumari B. S.: Synthesis of ZnO nanoparticles by a novel surfactant assisted amine combustion method. Advances in Nanoparticles, **2**, 45–50 (2013). https://doi.org/10.4236/anp.2013.21009

[91] Bernardo E., Fiocco L., Parcianello G., Storti E., Colombo P.: Advanced ceramics from preceramic polymers modified at the nano-scale: A review. Materials, **7**, 1927–1956 (2014). https://doi.org/10.3390/ma7031927

[92] Xu J. F., Ji W., Lin J. Y., Tang S. H., Du Y. W.: Preparation of ZnS nanoparticles by ultrasonic radiation method. Applied Physics A, **66**, 639–641 (1998). https://doi.org/10.1007/s003390050725

[93] Zhang H-B., Lin G-D., Zhou Z-H., Dong X., Chen T.: Raman spectra of MWCNTs and MWCNT-based H_2-adsorbing system. Carbon, **40**, 2429–2436 (2002). https://doi.org/10.1016/S0008-6223(02)00148-3

[94] Takamura A., Inoue K., Sakai T.: Resources recovery by pyrolysis of waste tyres. in 'First International Conference, Conversion of refuse to energy, Montreux, Switzerland' 532 (1975).

[95] Darmstadt H., Roy C., Kaliaguine S.: ESCA characterization of commercial carbon blacks and of carbon blacks from vacuum pyrolysis of used tires. Carbon, **32**, 1399–1406 (1944). https://doi.org/10.1016/0008-6223(94)90132-5

[96] Buekens A. G.: Some observations on the recycling of plastics and rubber. Conservation and Recycling, **1**, 247–271 (1977). https://doi.org/10.1016/0361-3658(77)90014-5

[97] Teng H., Li Y-U., Hsu L-Y.: Production of activated carbons from pyrolysis of waste tires impregnated with potassium hydroxide. Journal of the Air and Waste Management Association, **50**, 1940–1946 (2000). https://doi.org/10.1080/10473289.2000.10464221

[98] Ogasawara S., Kuroda O., Wakao N.: Preparation of activated carbon by thermal decomposition of used automotive tires. Industrial and Engineering Chemistry Research, **26**, 2552–2556 (1987). https://doi.org/10.1021/ie00072a030

[99] Sohn H. Y., Kim D.: Intrinsic kinetics of the reaction between zinc sulfide and water vapor. Metallurgical Transactions B, **18**, 451–457 (1987). https://doi.org/10.1007/BF02656166

[100] Medalia A. I.: Elastomers, reinforced of. in 'Encyclopedia of materials: Science and technology' (eds.: Buschow K. H. J., Flemings M. C., Kramer E. J., Veyssière P., Cahn R. W., Ilschner B., Mahajan S.) Pergamon, Oxford, 2475–2480 (2001). https://doi.org/10.1016/B0-08-043152-6/00447-2

[101] Frikha K., Limousy L., Claret J. P., Vaulot C., Pérez K. F., Corzo García B., Bennici S.: Potential valorization of waste tires as activated carbon-based adsorbent for organic contaminants removal. Materials, **15**, 1099 (2022). https://doi.org/10.3390/ma15031099

[102] Takesue M., Hayashi H., Smith R. L.: Thermal and chemical methods for producing zinc silicate (willemite): A review. Progress in Crystal Growth and Characterization of Materials, **55**, 98–124 (2009). https://doi.org/10.1016/j.pcrysgrow.2009.09.001

[103] Li Z. H., Zhang J., Chen S. J.: Effects of carbon blacks with various structures on vulcanization and reinforcement of filled ethylene-propylene-diene rubber. Express Polymer Letters, **2**, 695–704 (2008). https://doi.org/10.3144/expresspolymlett.2008.83

[104] Li D., Haneda H.: Morphologies of zinc oxide particles and their effects on photocatalysis. Chemosphere, **51**, 129–137 (2003). https://doi.org/10.1016/S0045-6535(02)00787-7

[105] Martínez J. D., Puy N., Murillo R., García T., Navarro M. V., Mastral A. M.: Waste tyre pyrolysis – A review. Renewable and Sustainable Energy Reviews, **23**, 179–213 (2013). https://doi.org/10.1016/j.rser.2013.02.038

[106] Straka P., Bičáková O., Šupová M.: Slow pyrolysis of waste polyethylene terephthalate yielding paraldehyde, ethylene glycol, benzoic acid and clean fuel. Polymer Degradation and Stability, **198**, 109900 (2022). https://doi.org/10.1016/j.polymdegradstab.2022.109900

[107] de D. López-González J., Velenzuela-Calahorro C., Navarrete-Guijosa A., Gómez-Serrano V.: Carbonization of olive wood: Evolution of surface area and porosity with treatment temperature. Adsorption Science and Technology, **3**, 41–48 (1986). https://doi.org/10.1177%2F026361748600300107

[108] Cunliffe A. M., Williams P. T.: Influence of process conditions on the rate of activation of chars derived from pyrolysis of used tires. Energy Fuels, **13**, 166–175 (1999). https://doi.org/10.1021/ef9801524

[109] Helleur R., Popovic N., Ikura M., Stanciulescu M., Liu D.: Characterization and potential applications of pyrolytic char from ablative pyrolysis of used tires. Journal of Analytical and Applied Pyrolysis, **58–59**, 813–824 (2001). https://doi.org/10.1016/s0165-2370(00)00207-2

[110] González J. F., Encinar J. M., González-García C. M., Sabio E., Ramiro A., Canito J. L., Gañan J.: Preparation of activated carbons from used tyres by gasification with steam and carbon dioxide. Applied Surface Science, **252**, 5999–6004 (2006). https://doi.org/10.1016/j.apsusc.2005.11.029

[111] Marzec M., Tryba B., Kaleńczuk R. J., Morawski A. W.: Poly(ethylene terephthalate) as a source for activated carbon. Polymers Advanced Technologies, **10**, 588–595 (1999). https://doi.org/10.1002/(SICI)1099-1581(199910)10:10%3C588::AID-PAT912%3E3.0.CO;2-H

[112] Handore K., Bhavsar S., Horne A., Chhattise P., Mohite K., Ambekar J., Pande N., Chabukswar V.: Novel green route of synthesis of ZnO nanoparticles by using natural biodegradable polymer and its application as a catalyst for oxidation of aldehydes. Journal of Macromolecular Science Part A, **51**, 941–947 (2014). https://doi.org/10.1080/10601325.2014.967078

[113] Lagergren S.: About the theory of so-called adsorption of soluble substances. Kungliga Svenska Vetenskapsakademiens. Handlingar, **24**, 1–39 (1898).

[114] Ho Y. S., McKay G.: Pseudo-second order model for sorption processes. Process Biochemistry, **34**, 451–465 (1999). https://doi.org/10.1016/S0032-9592(98)00112-5

[115] Giles C. H., MacEwan T. H., Nakhwa S. N., Smith D.: Studies in adsorption. Part XI. A system of classification of solution adsorption isotherms, and its use in diagnosis of adsorption mechanisms and in measurement of specific surface areas of solids. Journal of the Chemical Society, **1960**, 3973–3993 (1960). https://doi.org/10.1039/jr9600003973

[116] Kipling J. J., Wilson R. B.: Adsorption of methylene blue in the determination of surface areas. Journal of Applied Chemistrry, **10**, 109–113 (1960). https://doi.org/10.1002/jctb.5010100303

[117] Ardizzone S., Gabrielli G., Lazzari P.: Adsorption of methylene blue at solid/liquid and water/air interfaces. Colloids and Surfaces A: Physicochemical and Engineering Aspects, **76**, 149–157 (1993). https://doi.org/10.1016/0927-7757(93)80073-N

[118] Hang P. T., Brindley G. W.: Methylene blue absorption by clay minerals. Determination of surface areas and cation exchange capacities (clay-organic studies XVIII). Clays and Clay Minerals, **18**, 203–212 (1970). https://doi.org/10.1346/CCMN.1970.0180404

[119] de Souza Macedo J., da Costa Júnior N. B., Almeida L. E., da Silva Vieira E. F., Cestari A. R., Gimenez I. F., Carreño N. L. V., Barreto L. S.: Kinetic and calorimetric study of the adsorption of dyes on mesoporous activated carbon prepared from coconut coir dust. Journal of Colloid and Interface Science, **298**, 515–522 (2006). https://doi.org/10.1016/j.jcis.2006.01.021

[120] Langmuir I.: The adsorption of gases on plane surfaces of glass, mica and platinum. Journal of the American Chemical Society, **40**, 1361–1403 (1918). https://doi.org/10.1021/ja02242a004

[121] Freundlich H. M. F.: Über die Adsorption in Lösungen. Zeitschrift für Physikalische Chemie, **57**, 385–471 (1906). https://doi.org/10.1515/zpch-1907-5723

[122] Desta M. B.: Batch sorption experiments: Langmuir and Freundlich isotherm studies for the adsorption of textile metal ions onto teff straw (*Eragrostis tef)* agricultural waste. Journal of Thermodynamics, **2013**, 375830 (2013). https://doi.org/10.1155/2013/375830

[123] Jha V. K., Subedi K.: Preparation of activated charcoal adsorbent from waste tire. Journal of Nepal Chemical Society, **27**, 19–25 (2011). https://doi.org/10.3126/jncs.v27i1.6437

[124] Lian F., Xing B., Zhu L.: Comparative study on composition, structure, and adsorption behavior of activated carbons derived from different synthetic waste polymers. Journal of Colloid and Interface Science, **360**, 725–730 (2011). https://doi.org/10.1016/j.jcis.2011.04.103

[125] Makrigianni V., Giannakas A., Deligiannakis Y., Konstantinou I.: Adsorption of phenol and methylene blue from aqueous solutions by pyrolytic tire char: Equilibrium and kinetic studies. Journal of Environtal Chemical Engineering, **3**, 574–582 (2015). https://doi.org/10.1016/j.jece.2015.01.006

[126] Shaid M. S. H. M., Zaini M. A. A., Nasri N. S.: Isotherm studies of methylene blue adsorption onto waste tyre pyrolysis powder-based activated carbons. Malaysian Journal of Fundamental and Applied Sciences, **13**, 671–675 (2017). https://doi.org/10.11113/mjfas.v13n4.924

[127] Özbas E. E., Balcik B., Ozcan H. K.: Preparation of activated carbon from waste tires, and its use for dye removal. Desalination and Water Treatment, **172**, 78–85 (2019). https://doi.org/10.5004/dwt.2019.24493

[128] Djahed B., Shahsavani E., Naji F. K., Mahvi A. H.: A novel and inexpensive method for producing activated carbon from waste polyethylene terephthalate bottles and using it to remove methylene blue dye from aqueous solution. Desalination and Water Treatment, **57**, 9871–9880 (2016). https://doi.org/10.1080/19443994.2015.1033647

[129] de Castro C. S., Viau L. N., Andrade J. T., Prado Mendonça T. A., Gonçalves M.: Mesoporous activated carbon from polyethyleneterephthalate (PET) waste: Pollutant adsorption in aqueous solution. New Journal of Chemistry, **42**, 14612–14619 (2018). https://doi.org/10.1039/C8NJ02715C